Climate forcing and trends of organic aerosols in the Community Earth System Model (CESM2)

S. Tilmes[1], A. Hodzic[1], L. K. Emmons[1], M. J. Mills[1], A. Gettelman[1,2], D. E. Kinnison[1], M. Park[1], J.-F. Lamarque[2], F. Vitt[1], M. Shrivastava[3], P. Campuzano Jost[4,5], J. Jimenez[4,5], X. Liu[6].

[1]Atmospheric Chemistry, Observations, and Modeling Laboratory, National Center for Atmospheric Research, Boulder CO, USA

[2]Climate and Global Dynamics Laboratory, National Center for Atmospheric Research, Boulder CO, USA

[3]Atmospheric Sciences and Global Change Division, Pacific Northwest National Laboratory, Richland, WA, USA.

[4]Cooperative Institute for Research in Environmental Sciences (CIRES), University of Colorado, Boulder, CO, USA.

[5]Department of Chemistry, University of Colorado, Boulder, CO, USA.

[6]Department of Atmospheric Science, University of Wyoming, Laramie, Wyoming, USA.

Key Points:

- CESM2(WACCM6) includes an updated secondary aerosol scheme using the Volatility Basis Set approach
- The new SOA parameterization results in regional changes in radiative forcings and aerosol optical depth
- SOA trends are increasing between 1960-2015 with contributions from biogenic and anthropogenic sources

Corresponding author: Simone Tilmes, `tilmes@ucar.edu`

Abstract

The Community Earth System Model version 2 (CESM2) includes three main atmospheric configurations, the Community Atmosphere Model version 6 (CAM6), CAM6 with comprehensive tropospheric and stratospheric chemistry representation (CAM6-chem), and the Whole Atmosphere Community Climate Model version 6 (WACCM6). This paper describes the organic aerosol (OA) schemes available in the different atmospheric configurations of CESM2 and discusses differences in aerosol burden and resulting climate forcings. Large regional differences in radiative forcing and Aerosol Optical Depth (AOD) occur between model versions that use the simplified aerosol and chemistry description compared to model configurations that include prognostic stratospheric aerosols and a more comprehensive secondary organic aerosol (SOA) parameterization including the Volatility Basis Set (VBS) approach. Using the comprehensive SOA approach, OA in WACCM6 agree within $\approx 20\%$ with aircraft observations over remote regions, which is improved compared to the simplified parameterization. The predicted SOA formation is ≈ 143 Tg per year, which is in close agreement with observationally constrained estimates. We further use WACCM6 to identify source contributions of OA from biogenic, fossil fuel, and biomass burning emissions, to quantify SOA amounts and trends from these sources. Increasing SOA trends between 1960–2015 are the result of increasing biogenic emissions aligned with increasing surface temperatures, which contribute at least two thirds to the total SOA burden. In addition, SOA source contributions from fossil fuel emissions become more important, with largest values over Southeast Asia. The estimated total anthropogenic forcing of OA in WACCM6 for 1995–2010 conditions is 0.43 W/m^2, mostly from the aerosol direct effect.

1 Introduction

Organic aerosols (OA) are important climate forcers and contribute to reduced air quality in many regions, but have not been well represented in climate models. Parameterizations of OA in Earth System Models are often rather simplified. Amounts of the derived OA differ largely between different models and underestimate observational estimates in remote regions [*Tsigaridis et al.*, 2014]. This is in part because the complex formation processes of OA through oxidative chemistry from various precursors [e.g., *Pandis et al.*, 1991] are not sufficiently well represented. There is also still an incomplete understanding of the composition, aging, deposition, radiative absorption, and other pro-

cesses in the atmosphere [*Hallquist et al.*, 2009; *Heald et al.*, 2011; *Hodzic et al.*, 2016; *Shrivastava et al.*, 2017; *Tsigaridis and Kanakidou*, 2018, and references therein]. Organic aerosols are important short-lived climate forcers due to their direct effect in scattering and reflecting sunlight, their radiative warming effects through light absorption in particular from brown carbon [*Zhang et al.*, 2017], and indirectly through interactions with clouds [*Carslaw et al.*, 2013; *Hodzic and Duvel*, 2018]. Due to the insufficient description in many climate models there is a large uncertainty in the magnitude of the radiative effects of OA.

OA can be classified into two types: primary and secondary. The primary type, known as Primary Organic Matter (POM), is directly emitted from fossil fuel combustion and biomass burning. POM undergoes transport, chemical aging, and eventual removal by dry and wet deposition. In addition, POM can evaporate, and further oxidize to form Secondary Organic Aerosols (SOA) [*Robinson et al.*, 2007; *Hodzic et al.*, 2010; *Jathar et al.*, 2014]. The dominant sources of SOA are precursor emissions of Volatile Organic Compounds (VOC). Biogenic VOC emissions in the model include isoprene and monoterpenes, emissions from biomass burning and anthropogenic sources include aromatics and linear and branched hydrocarbons. The oxidation of these gaseous precursors, mainly with OH radicals and ozone (O_3) during the day and nitrate radicals (NO_3) at night, leads to the formation of hundreds of semi-volatile condensable organics that can condense to form SOA. The processing of these gases depends on the atmospheric composition, in particular the concentrations of oxidants (OH, ozone) and NO_x [*Hallquist et al.*, 2009]. These gas-phase semi-volatile condensable sources of SOA are referred to as SOAG herein.

Global climate models cannot fully represent the complex tropospheric chemistry that would allow for a comprehensive description of organic aerosol (OA) formation in the same way as included in process models, because of computational limitations. Explicit mechanisms represent reactivity of organic carbon in various phases down to the ultimate oxidation products, CO and CO_2, and include thousands of species and reactions [*Aumont et al.*, 2005]. Simplified parameterizations to represent OA of various complexity have been implemented into GCMs in recent years. For POM, often very simple descriptions based on emissions, chemical aging, and deposition, have been implemented [*Liu et al.*, 2012, 2016]. For SOA, one of the simpler approaches uses prescribed SOAG emission fluxes that are directly proportional to the emissions of precursors [e.g., *Chin et al.*, 2002; *Colarco et al.*, 2010; *Liu et al.*, 2012, 2016], or an empirically deter-

mined emission flux scaled to CO emissions [*Hodzic et al.*, 2010; *Spracklen et al.*, 2011]. Another frequently used approach is the two-product SOA representation as used in earlier CESM configurations [e.g., *Heald et al.*, 2011; *Tilmes et al.*, 2016]. This approach includes the oxidation of precursors into two condensable organic products that can form SOA [*Odum et al.*, 1996]. *Tsigaridis et al.* [2014] showed that these commonly used approaches in ≈ 30 global models that participated in the AeroCom-II intercomparison led to a substantial underprediction of surface SOA concentrations near source regions.

Currently, one of the most advanced parameterization in global models is the Volatility Basis Set (VBS) scheme, which groups hundreds of intermediate semi-volatile organic compounds by bins of volatility that are produced by oxidative chemistry from the emitted precursors [*Donahue et al.*, 2006; *Tsimpidi et al.*, 2010; *Shrivastava et al.*, 2013; *Hodzic et al.*, 2016]. VBS parameterizations are typically adjusted to reproduce the SOA formation yields in chamber experiments for various individual precursors and atmospheric conditions [e.g., *Ng et al.*, 2007]. The VBS implementation into global models can, however, vary significantly as it is based on different sets of chamber data and their interpretation. For instance, VBS parameterizations can be based on traditional chamber data that suffer from wall losses [*Pye and Seinfeld*, 2010], or modified to account for further aging of organics in the atmosphere beyond chamber timescales [*Shrivastava et al.*, 2015], or adjusted to wall-loss corrected chamber data [*Hodzic et al.*, 2016]. This latter scheme has been shown to reproduce SOA budgets and distributions fairly well in a global model [*Hodzic et al.*, 2016].

In this paper, we compare two different representations of OA that are available in CESM2. For the standard CESM2 version, the Community Atmosphere Model (CAM6) uses a simplified SOA formation description [*Liu et al.*, 2012, 2016]. SOAG yields are directly derived from emissions and emitted without the consideration of continuous chemical formation processes. CESM2 versions with extended chemistry, as used in the CAM6 with chemistry, CESM2-CAM6-chem (hereafter CAM6-chem), and in the Whole Atmosphere Community Climate model CESM2-WACCM6 (hereafter WACCM6), have been updated to the more sophisticated SOA approach. This approach, based on *Hodzic et al.* [2016], includes the VBS scheme for simulating SOA formation, as well as additional processes, as described below. The new SOA description in WACCM6 and CAM6-chem also allows separating of precursor emissions from biogenic, anthropogenic (or fossil fuel) and

biomass burning sources, to be able to identify the importance of different sources of SOA formation in past, present and future climates.

The model description and different OA parameterizations in CESM2 and experiments performed for this study are described in Section 2. In Section 3, results from different model configurations are compared, including differences in aerosol burden, SOA formation, deposition, lifetime, and differences in radiative forcing. In addition, comparisons of OA to observations are performed. OA in the remote troposphere are evaluated using observations from the NASA ATom aircraft mission [*Wofsy et al.*, 2018]. In Section 4, the time evolution of SOA source contributions from separate precursors over selected regions are summarized. We discuss the importance of anthropogenic precursor emissions to the total SOA burden and quantify the effects on radiation. Discussions and conclusions are presented in Section 5.

2 Model Description and Experiments

2.1 Model Description

The experiments performed in this study are all based on the CESM2.0 release version. Some minor updates were performed between CESM2.0 and CESM2.1, with the latter version being used for CMIP6 simulations. Those changes have no impact on the results or conclusions of this paper. In CESM2, the WACCM6 and CAM6 setups are as similar as possible with the intention to achieve a similar climate outcome with the two versions of the model [*Gettelman et al.*, 2019]. The high-top (WACCM6) and low-top (CAM6 and CAM6-chem) configurations of CESM2 include the same atmospheric physics in the troposphere. They only differ in a few specifications, including the vertical grid, required gravity wave additions in WACCM6, and structure of the so-called "sponge-layer" at the CAM6 model top. While WACCM6 uses 72 vertical layers up to about 150 km, CAM6 only uses 32 vertical layers and reaches vertically up to about 1 hPa (40 km). Furthermore, WACCM6 includes convective, frontal, and orographic sources of gravity waves, which propagate to drive the circulation of the middle atmosphere, CAM6 includes only orographic sources. As a result, CAM6 has a degraded stratospheric circulation compared to WACCM6. Both WACCM6 and CAM6 configurations use a 0.95° in latitude by 1.25° in longitude horizontal grid. Two WACCM6 experiments presented in this paper were performed with the specified dynamics (SD) version of WACCM6, whereby the winds,

temperature and surface fluxes are nudged towards NASA GMAO GEOS5.12 meteorological analysis with a Newtonian relaxation of 50 hours for the years 2016-2017, for comparisons with observations. The SD version of the model adopts the levels of GEOS5 below 50 km, and has a total of 88 vertical levels reaching to the model top.

The standard version of WACCM6 uses comprehensive troposphere, stratosphere, mesosphere and lower thermosphere chemistry, also called TSMLT. A specified chemistry configuration of WACCM6, called WACCM6-SC, has been used to represent simplified chemistry and a simple SOA parameterization, similar to standard CAM6 [*Gettelman et al.*, 2019]. Both, WACCM6-SC and CAM6 use the simple SOA parameterization with a single lumped semi-volatile organic gas-phase species, called SOAG, since the simplified chemistry does not include the oxidation of VOCs. The pre-processed surface emissions of SOAG are derived from emission datasets of five primary VOCs, using the following mass yields: 5% BIGALK (lumped butanes and larger alkanes), 5% BIGENE (lumped butenes and larger alkenes), 15% aromatics, 4% isoprene, 25% monoterpenes [*Liu et al.*, 2012]. SOAG undergoes condensation and evaporation into the Aitken and accumulation modes of the Modal Aerosol Model (MAM). These processes dependent on the gas saturation vapor concentration, temperature, and POM concentration, 10% of which is assumed to be oxygenated [*Liu et al.*, 2012]. As in CESM1, SOAG emissions have been increased by a factor of 1.5 [*Liu et al.*, 2012] and SOAG does not undergo dry and wet removal. We call this simplified approach the "SOAG scheme".

WACCM6 and CAM6-chem include a comprehensive SOA parameterization based on the VBS model framework following the approach by *Hodzic et al.* [2016]. The parameterization is based on chamber measurements and explicit modeling, as briefly summarized next. The scheme includes both updates to the SOA formation and removal pathways. In terms of SOA formation, semi-volatile SOAGs are produced from anthropogenic and biomass burning precursor emissions at the surface, as well as biogenic emissions from the Model of Emissions of Gases and Aerosols from Nature (MEGAN) version 2.1 [*Guenther et al.*, 2012]. For traditional precursors (biogenic VOCs, aromatics and short-chain alkanes), the required parameters for applying the VBS scheme were fitted to the wall-corrected chamber data, performed in the Caltech chambers, as summarized in *Zhang et al.* [2014], and extrapolated to longer times beyond the duration of the experiment. SOA formation from the oxidation of long-chain n-alkanes emitted from fossil-fuel, biofuel, and biomass burning sources is considered [e.g., *Robinson et al.*, 2007; *Gentner et al.*,

Table 1. Reactions added to represent molar yields from different SOA precursors. These are dependent on volatility and binned into logarithmically spaced bins (see text for more detail).

Reactions				Rates
XYLENES + OH	→	XYLENES + OH + 0.1677*SOAGff0 + 0.0174*SOAGff1 + 0.0860*SOAGff2 + 0.0512*SOAGff3 + 0.1598*SOAGff4	;	1.7e-11
TOLUENE + OH	→	TOLUENE + OH + 0.1364*SOAGff0 + 0.0101*SOAGff1 + 0.0763*SOAGff2 + 0.2157*SOAGff3 + 0.0738**SOAGff4	;	1.7e-12*exp(352./t)
BENZENE + OH	→	BENZENE + OH +0.0023*SOAGff0 + 0.0008*SOAGff1 + 0.0843*SOAGff2 + 0.0443*SOAGff3 + 0.1621*SOAGff4	;	2.3e-12*exp(-193./t)
ISOP + NO3	→	ISOP + NO3 + 0.059024*SOAGbg3 + 0.025024*SOAGbg4	;	3.03e-12*exp(-446./t)
ISOP + O3	→	ISOP + O3 + 0.0033*SOAGbg3	;	1.05e-14*exp(-2000./t)
ISOP + OH	→	ISOP + OH + 0.0031*SOAGbg0 + 0.0035*SOAGbg1 + 0.0003*SOAGbg2 + 0.0271*SOAGbg3 + 0.0474*SOAGbg4	;	2.54e-11*exp(410./t)
BCARY + NO3	→	BCARY + NO3 + 0.17493*SOAGbg3 + 0.59019*SOAGbg4	;	1.9e-11
BCARY + O3	→	BCARY + O3 + 0.2202*SOAGbg0 + 0.2067*SOAGbg1 + 0.0653*SOAGbg2 + 0.1284*SOAGbg3 + 0.114*SOAGbg4	;	1.2e-14
BCARY + OH	→	BCARY + OH + 0.2202*SOAGbg0 + 0.2067*SOAGbg1 + 0.0653*SOAGbg2 + 0.1284*SOAGbg3 + 0.114*SOAGbg4	;	2e-10
MTERP + NO3	→	MTERP + NO3 + 0.17493*SOAGbg3 + 0.59019*SOAGbg4	;	1.2e-12, 490
MTERP + O3	→	MTERP + O3 + 0.0508*SOAGbg0 + 0.1149*SOAGbg1 + 0.0348*SOAGbg2 + 0.0554*SOAGbg3 + 0.1278*SOAGbg4	;	6.3e-16*exp(-580./t)
MTERP + OH	→	MTERP + OH + 0.0508*SOAGbg0 + 0.1149*SOAGbg1 + 0.0348*SOAGbg2 + 0.0554*SOAGbg3 + 0.1278*SOAGbg4	;	1.2e-11*exp(440./t)
IVOCbb + OH	→	0.2381*SOAGbb0 + 0.1308*SOAGbb1 + 0.0348*SOAGbb2 + 0.0076*SOAGbb3 + 0.0113*SOAGbb4+ OH	;	1.34e-11
SVOCbb + OH	→	0.5931*SOAGbb0 + 0.1534*SOAGbb1 + 0.0459*SOAGbb2 + 0.0085*SOAGbb3 + 0.0128*SOAGbb4+ OH	;	1.34e-11
IVOCff + OH	→	0.2381*SOAGff0 + 0.1308*SOAGff1 + 0.0348*SOAGff2 + 0.0076*SOAGff3 + 0.0113*SOAGff4+ OH	;	1.34e-11
SVOCff + OH	→	0.5931*SOAGff0 + 0.1534*SOAGff1 + 0.0459*SOAGff2 + 0.0085*SOAGff3 + 0.0128*SOAGff4+ OH	;	1.34e-11
GLYOXAL	→	SOAGbg0		

2012]. The formation of semi volatile organic carbons (SVOC) are assumed as being produced from 60% of POM emissions; intermediate volatility organic carbons (IVOC) are assumed to be produced from 20% of NMVOC emissions (not including SVOC emissions). These precursor emissions were oxidized into SOAGs in each volatility bin (see Table 1).

For long-chain n-alkane (number of carbons > 12) precursors species, VBS parameters were derived from the simulations of an explicit chemical model performed for n-alkanes mixtures. Parameters were derived for both low and high NO_x conditions. Currently, only low NO_x conditions are considered CESM2, which is appropriate for a coarse horizontal resolution of the model grid. However, especially for finer horizontal resolutions than used here, shortcomings of this assumption may exist for highly polluted regions over large cities as well as regions that experience intensive biomass burning.

In contrast to the implementation described by *Hodzic et al.* [2016], the SOAG product species in CESM2 are binned by their saturation concentration (C^*) into 5 instead of 6 logarithmically spaced bins (of 0.01, 0.1, 1., 10. and 100 μg m^{-3} at 300K). This has been done by lumping together the two most volatile bins with the purpose of reducing computational costs. The resulting products are called SOAG0, SOAG1, SOAG2, SOAG3, SOAG4 in the model. The isoprene oxidation with ozone only produces a gas product in the volatility of 10 μg m^{-3} (SOAG3) based on *Kleindienst et al.* [2007].

With the new parameterization, the importance of different precursor emissions on SOA can be investigated using an extended version of the released model, the so called "extended VBS (VBSext)" version of WACCM6, or WACCM6-VBSext. Depending on their precursor emissions, the products are separated into SOAGff (for fossil fuel), SOAGbb (for biomass burning), and SOAGbg (for biogenic) for WACCM6-VBSext. Likewise, POM species have been separated into POMff and POMbb in WACCM6-VBSext. For the standard VBS version in WACCM6, SOAG yields are not separated by precursor sources to reduce computational costs. For the formation of SOAG from different precursor emissions, all the mass yields listed in *Hodzic et al.* [2016] have been converted to molar yields (Table 1).

In addition to the VBS formation scheme, dry and wet deposition for all intermediate VBS gaseous SOAG species was added, and depends on the hygroscopicity of organic gaseous species. The water solubility of gaseous species is given as a function of volatility following *Hodzic et al.* [2014]. Furthermore, the photolytic removal of partic-

ulate SOA has also been included with a value for J_{SOA} of $0.04 \times J_{NO_2}$, as discussed in *Hodzic et al.* [2015, 2016], and the SOA formation from glyoxal in aqueous aerosols is considered based on *Knote et al.* [2014].

The new SOA parameterization has only been applied to CESM2 model configurations that include comprehensive tropospheric chemistry, WACCM6 and CAM6-chem. The description of the diurnal cycle and interactive chemistry of precursors and oxidants are important for the SOA production. For this study, an additional model configuration has been developed in order to determine the impact of the advanced SOA scheme in WACCM6. This so called WACCM6-SOAG configuration includes fully interactive aerosol and chemistry, the same as WACCM6, however, the simplified SOA scheme has been implemented as used in WACCM6-SC and CAM6. This setup does not include the VBS scheme, or any of the additions listed above.

In addition to the differences in the OC description in the different model versions, prognostic stratospheric sulfate aerosols are included in configurations that run with the comprehensive chemistry. Carbonyl sulfide (OCS), an important non-volcanic source of stratospheric sulfate, has been added to the chemical mechanism [*Mills et al.*, 2017]. Dimethyl sulfide (DMS) is largely emitted from oceans, as well as to a small extent from biomass burning and adds an additional source of tropospheric sulfate aerosols in WACCM6. Changes in the sulfate aerosol burden are discussed in this paper, since they are important for discussing differences in the radiative forcings between the different CESM2 configurations.

2.2 Model Experiments

CESM2.0 has been used to perform 13 different experiments using configurations of different complexity (as listed in Table 2). All the model simulations are performed with observed sea-surface temperatures and sea-ice conditions. The first set of 5 experiments were performed for pre-industrial (PI) conditions, with emissions and lower boundary conditions (greenhouse gas concentrations) fixed to levels from the year 1850. PI experiments with TSMLT chemistry include constant time-averaged stratospheric emissions from eruptions over the historical period (1850-2014), in order to impose an average forcing from volcanic eruptions reaching the stratosphere. The second set of experiments started from 1960 spun-up conditions (with a spin-up time of at least 10 years each) and continued until the end of 2014. For these experiments CMIP6 emissions and

Table 2. Overview of simulations for pre-industrial and present-day conditions and specified dynamics (SD). All simulations have used observed sea surface temperatures. The names of existing configuration sets in CESM2 that correspond to a specific experiment are listed in brackets.

Configuration (Compset)	years	SOA model	Sulfate	Chemistry
WACCM6 (FW1850)	1850 (10)	standard VBS	PI avg. prognostic	TSMLT
WACCM6-VBSext (FWvbsx1850)	1850 (10)	extended VBS	PI avg. prognostic	TSMLT + OA sources
WACCM6-SOAG	1850 (10)	simplified SOA	PI avg. prognostic	TSMLT
WACCM6-SC (FWsc1850)	1850 (10)	simplified SOA	PI avg. prescribed strat.	simple chemistry
CAM6 (F1850)	1850	simplified SOA	PI avg. prescribed strat	simple chemistry
WACCM6 (FWHIST)	1960-2014	standard VBS	prognostic	TSMLT
WACCM6-VBSext (FWvbsxHIST)	1960-2014	extended VBS	prognostic	TSMLT + OA sources
WACCM6-NA	1960-2014	extended VBS	prognostic	TSMLT + OA sources (no anthro)
WACCM6-SOAG	1960-2014	simplified SOA	prognostic	TSMLT
WACCM6-SC (FWscHIST)	1960-2014	simplified SOA	prescribed strat.	simple chemistry
CAM6 (FHIST)	1960-2014	simplified SOA	prescribed strat	simple chemistry
WACCM6-VBSext (FWSDvbsxHIST)	2016-2017 (SD)	extended VBS	prognostic	TSMLT + OA sources
WACCM6-SOAG	2016-2017 (SD)	simplified SOA	prognostic	TSMLT + OA sources

surface concentrations for the historical period have been used [*Hoesly et al.*, 2018]. The transient model experiments with TSMLT chemistry include the SO_2 emissions from volcanic eruptions, based on version 3.11 of Volcanic Emissions for Earth System Models (VolcanEESM) [*Neely, R. R. and Schmidt*, 2016], as described in *Gettelman et al.* [2019]. For all WACCM6-SC and CAM6 experiments performed here, prescribed ozone, oxidants and stratospheric aerosol datasets are derived from the corresponding WACCM6 experiments.

One additional transient WACCM-VBSext experiment has been performed without any anthropogenic OA contributions, called WACCM-NoAnthro, or short WACCM-NA from here on. This experiment does include all SOA formation processes and POM emissions besides those from anthropogenic sources (i.e. benzene, toluene, xylenes, and long-chain n-alkane). In this way, the gas-phase chemistry has not changed compared to the standard WACCM simulation, and only the formation of anthropogenic SOAG has been removed. The purpose of this experiment is to identify the impact and radiative forcings of SOA from anthropogenic sources, as further discussed in Section 4.

The two SD experiments (using WACCM6-VBSext and WACCM6-SOAG configurations) were performed for the years 2016 and 2017 to reproduce the observed meteorological conditions and to allow a direct comparison with results from ATom aircraft observations [*Wofsy et al.*, 2018]. These experiments use anthropogenic CMIP6 emissions from the year 2014, and daily fire emissions for 2016 and 2017 from QFED [*Darmenov et al.*, 2015], prepared by using the QFED CO_2 fields, multiplied by the species emissions factors collated in Fire INventory from NCAR Version 1.5 (FINNv1.5) [Table S1 at http://bai.acom.ucar.edu/Data/fire/] [*Wiedinmyer et al.*, 2011].

3 Aerosol burden and radiative forcings for different CESM2 configurations

The main differences between CAM6 and WACCM6, besides the model top, is the description of chemistry and aerosols that leads to differences in radiative forcings. Here we explore the importance of differences between CESM2 configurations on aerosol burden and distribution in the model and the effects on radiation. In addition, a comparison of OA to observations is performed to identify improvements in using configurations with a comprehensive SOA parameterization.

First, we compare results derived from standard WACCM6 and WACCM6-VBSext (Figure 1, black and blue lines, and Tables 3 and 4). In WACCM6-VBSext, SOAGs from biogenic sources use slightly different values of water solubility than those from biomass burning and fossil fuel emissions [*Hodzic et al.*, 2014]. In the WACCM6 standard version, SOAG are lumped together and an average value is used for all of them. Only very small differences (less than 1%) in wet and dry deposition and aerosol formation exist between the two versions. Differences in aerosol burden are within the internal variability of the model and are therefore not further discussed. In conclusion, the simplified VBS scheme is giving the same results for lower computational costs (around 15% less) than the extended VBS version, and can be used for simulations where information of SOA precursor sources is not required, for instance for long climate simulations.

3.1 Changes based on the new SOA VBS aerosol scheme

To understand the benefits of using the updated comprehensive SOA scheme compared to the fixed yield SOAG scheme, we compare simulations with and without the VBS scheme, in particular we compare WACCM6-VBSext and WACCM6-SOAG. WACCM6-SOAG and configurations that include the simplified SOA scheme like CAM6 and WACCM6-SC, show consistently larger SOA burden for PI conditions of around 15-20% (Table 3). On the other hand, values of SOA burden agree between WACCM6 and WACCM6-SOAG for present day at around 1.05 Tg for all the configuration (Table 4, and Figure 1). Resulting trends in SOA burden between PI conditions and present day are therefore different in the two configurations leading to a 20% increase in SOA for WACCM6 and WACCM6-VBSext and less than 10% increase for WACCM6-SOAG and other experiments using the simplified SOA schemes. The two schemes are therefore expected to result in a different response to changes in climate.

Differences in aerosol burden, deposition, SOA formation, and lifetime (Tables 3 and 4) between these different approaches arise from the very different way SOAG formation is described in both approaches, considerations of SOAG removal through dry and wet deposition, and the considered glyoxal uptake. For the simplified SOA scheme, SOAG is emitted at the surface and will go through gas-to-aerosol partitioning immediately, while for the VBS approach, SOAG is formed from precursor emissions while reacting with OH, O_3 and NO_3, resulting in changes in the temporal and spatial aerosol distributions. In particular, larger SOA mass mixing ratio in the upper tropical tropo-

288 **Table 3.** Averaged aerosol burden for pre-industrial conditions.

Model	WACCM6	WACCM6	WACCM6	WACCM6	CAM6
Chemistry	TSMLT	TSMLT	TSMLT	SC	SC
SOA	VBS	VBS-ext	SOAG	SOAG	SOAG
POM BURDEN (Tg)	0.40	0.40	0.51	0.52	0.51
biomass burning (Tg)		0.31			
fossil fuel (Tg)		0.09			
POM EMIS (Tg/yr)	25.79	25.79	25.79	25.79	25.79
POM DRYDEP (Tg/yr)	8.74	8.73	9.67	9.70	9.20
POM WETDEP (Tg/yr)	17.06	17.07	16.13	16.10	16.06
POM LIFETIME (days)	5.64	5.69	7.23	7.28	7.40
BC BURDEN (Tg)	0.042	0.042	0.051	0.051	0.051
BC EMIS (Tg/yr)	2.60	2.60	2.60	2.60	2.60
BC DRYDEP (Tg/yr)	0.88	0.87	0.95	0.96	0.92
BC WETDEP (Tg/yr)	1.72	1.72	1.64	1.64	1.64
BC LIFETIME (days)	5.85	5.90	7.13	7.19	7.26
SOA BURDEN (Tg)	0.78	0.78	0.90	0.92	0.94
biomass burning (Tg)		0.08			
biogenic (Tg)		0.67			
fossil fuel (Tg)		0.04			
SOA Formation (Tg/yr)	101.01	101.78	69.26	69.26	67.17
SOA DRYDEP (Tg/yr)	6.78	6.825	11.14	11.01	8.39
SOA WETDEP (Tg/yr)	48.32	48.942	58.14	58.26	58.78
SOA Photolysis (Tg/yr)	45.65	46.01	0.00	0.00	0.00
SOA LIFETIME (days)	5.156	5.134	4.748	4.823	5.12
SO4 BURDEN (<500hPa) (TgS)	0.084	0.085	0.084	0.075	0.076
SO4 Formation (TgS/yr)	0.39	0.39	0.39	0.39	0.39
SO4 DRYDEP (TgS/yr)	1.41	1.43	1.41	1.29	0.97
SO4 WETDEP (TgS/yr)	10.83	10.86	10.88	10.39	10.44
SO4 CHMP (TgS/yr)	11.85	11.90	11.90	11.29	11.02
SO4 LIFETIME (<500hPa) (days)	2.49	2.52	2.51	2.34	2.42
DUST BURDEN (Tg)	26.28	27.36	26.80	26.59	26.66
SALT BURDEN (Tg)	8.67	8.72	8.68	8.60	8.76

289 **Table 4.** Averaged aerosol burden for 1995-2010 conditions.

Model	WACCM6	WACCM6	WACCM6	WACCM6	CAM6	WACCM6
Chemistry	TSMLT	TSMLT	TSMLT	SC	SC	TSMLT
SOA	VBS	VBS-ext	SOAG	SOAG	SOAG	VBS-ext
POM BURDEN (Tg)	0.74	0.74	0.93	0.93	0.94	0.41
biomass burning (Tg)		0.39				0.41
fossil fuel (Tg)		0.35				0.00
POM EMIS (Tg/yr)	46.20	46.20	46.20	46.20	46.20	23.91
POM DRYDEP (Tg/yr)	13.36	13.36	14.20	14.15	13.38	7.04
POM WETDEP (Tg/yr)	32.84	32.83	32.00	32.05	32.01	16.88
POM LIFETIME (days)	5.85	5.85	7.34	7.35	7.56	6.26
BC BURDEN (Tg)	0.13	0.13	0.15	0.15	0.15	0.13
BC EMIS (Tg/yr)	8.47	8.47	8.47	8.46	8.46	8.47
BC DRYDEP (Tg/yr)	2.53	2.53	2.60	2.58	2.44	2.87
BC WETDEP (Tg/yr)	5.94	5.94	5.88	5.88	5.87	5.60
BC LIFETIME (days)	5.60	5.60	5.46	5.47	6.59	5.60
SOA BURDEN (Tg)	1.04	1.05	1.03	1.04	1.07	0.78
Biomass Burning (Tg)		0.10				0.10
Biogenic (Tg)		0.70				0.68
Fossil fuel (Tg)		0.25				0.00
SOA Formation (Tg/yr)	142.18	143.44	79.45	79.45	77.39	106.08
SOA DRYDEP (Tg/yr)	12.28	12.50	13.56	13.55	10.76	8.36
SOA WETDEP (Tg/yr)	72.10	72.96	65.90	65.91	66.63	53.75
SOA Photolysis (Tg/yr)	57.48	57.98	0.00	0.00	0.00	43.97
SOA LIFETIME (<500hPa) (days)	4.49	4.48	4.74	4.77	5.04	4.56
SO4 BURDEN (<500hPa) (TgS)	0.29	0.29	0.29	0.27	0.27	0.29
SO4 Formation (TgS/yr)	1.81	1.81	1.81	1.81	1.81	1.81
SO4 DRYDEP (TgS/yr)	4.98	4.93	4.99	4.88	3.70	5.08
SO4 WETDEP (TgS/yr)	31.27	31.22	31.28	30.47	30.44	31.18
SO4 TOTAL PROD (TgS/yr)	34.45	34.34	34.46	33.543	32.33	34.44
SO4 LIFETIME (<500hPa) (days)	2.92	2.93	2.92	2.79	2.89	2.91
DUST BURDEN (Tg)	25.91	25.97	25.87	25.43	26.77	26.54
Sea-salt BURDEN (Tg)	8.91	8.90	8.87	8.84	8.92	8.86

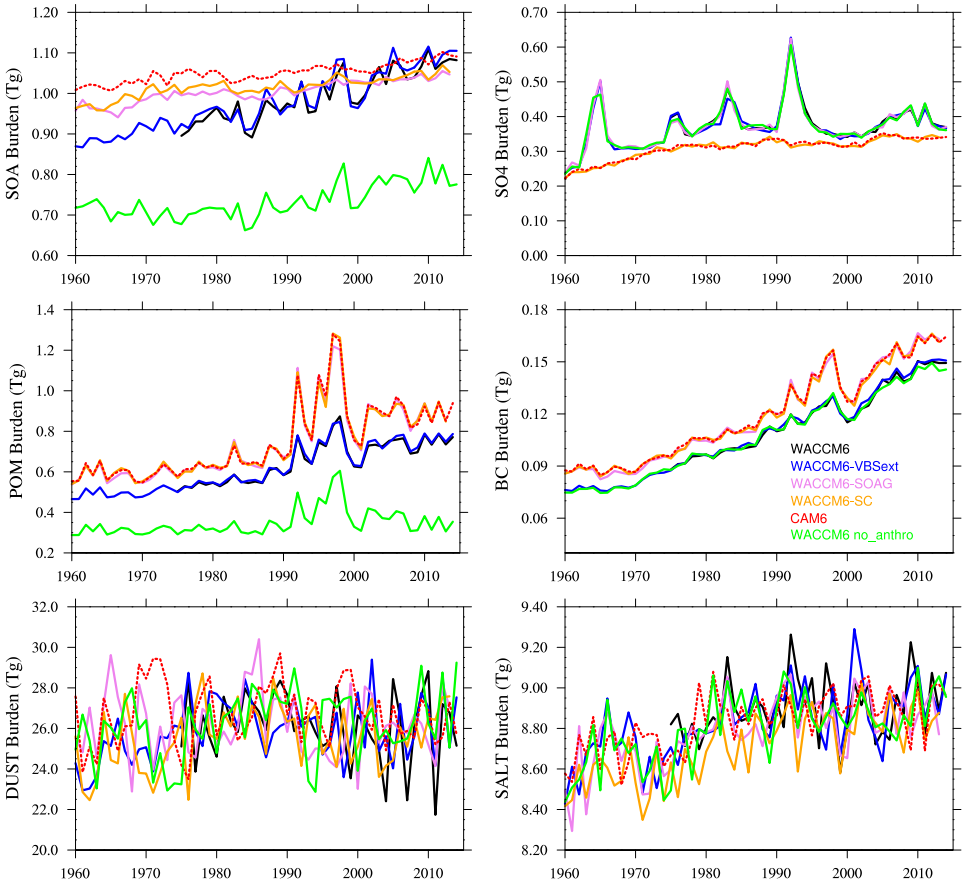

Figure 1. Annually and globally averaged aerosol burdens for simulations (see legend, and Table 2), SOA (top left), SO_4 only for altitudes below 500hPa (top right), POM (middle left), BC (middle right), dust (bottom left), and sea-salt (bottom right).

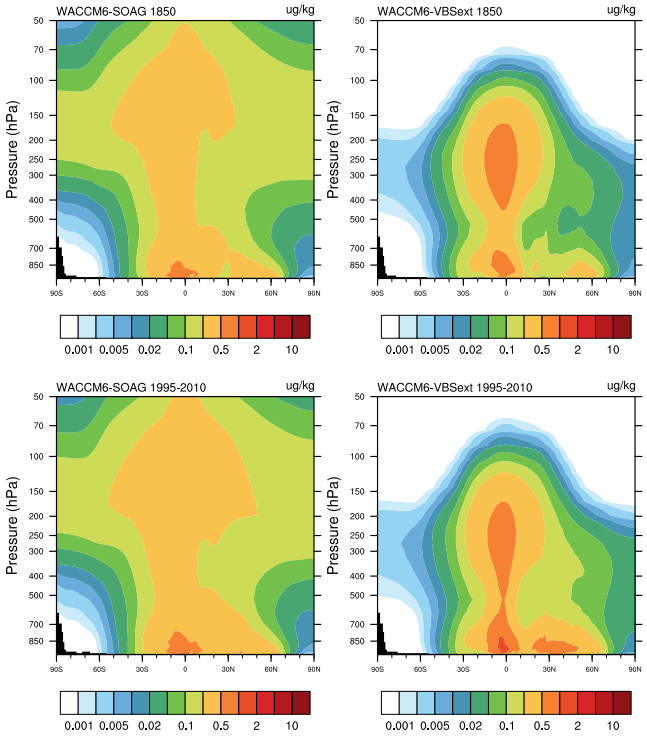

306 **Figure 2.** Secondary Organic Aerosol (SOA) zonal and annual mean distribution for
307 WACCM6-SOAG (left) and WACCM6-VBSext (right), averaged over 10 years for preindustrial
308 conditions (top) and between 1995-2010 (bottom).

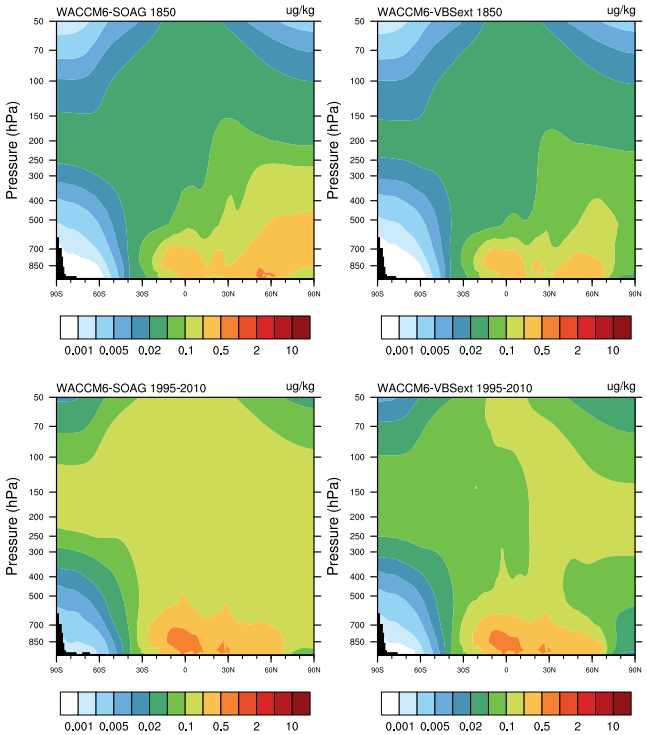

309 **Figure 3.** As Figure 2, but instead for Primary Organic Matter (POM).

sphere in WACCM6-VBSext compared to WACCM6-SOAG (as shown in Figure 2) is the result of the slower formation processes of SOA near the surface due to chemical processing for both PI conditions and present day. Furthermore, the reduced SOA levels in stratosphere and high latitudes in WACCM6-VBSext is likely a result of the additionally included photolytic removal of SOA and the deposition of SOAG.

Changes in SOA formation between WACCM6-SOAG and WACCM6-VBSext also affect POM and BC (Figure 1, middle row, Figure 3). POM and BC global burdens are consistently larger in WACCM6-SOAG compared to WACCM6-VBSext; POM and BC are more than 20% larger for PI and somewhat less for present day. The zonal average distribution of POM shows larger values in the upper troposphere and in particular at high latitudes in WACCM6-SOAG compared to WACCM6-VBSext (Figure 4). The reason for changes in POM and BC (not shown) are linked to a strong increase of SOA formation over source regions using the VBS scheme in WACCM6-VBSext. In all the model configuration, POM and BC are emitted into the primary organic (hydrophobic) mode, and slowly age into the accumulation model through condensation and coagulation, with a threshold coating thickness of 8 hygroscopic monolayers of SOA [*Liu et al.*, 2016]. The enhancement of SOA increases the internally mixed aerosol number that causes enhanced aging of POM and BC (see Tables 5 and 6). The primary carbon (hydrophobic) mode of POM and BC in the model is over 50% larger when using the SOAG scheme compared to configurations using the VBS scheme, while the accumulation mode (hydrophilic) is about 10% smaller. This results in increased dry deposition and decreased wet deposition in WACCM6-SOAG, and therefore in larger POM and BC burdens. Increasing mixing ratios are in particular pronounced in the northern mid- and high latitudes. Smaller burdens in the accumulation mode also occur for sulfate aerosols (SO_4), with a larger coarse mode burden in WACCM6-SOAG. These differences seem to have very little impact on the total SO_4 burden for PI or PD conditions (Tables 5 and 6). Dust and sea-salt are also not impacted by the different SOA parameterizations (Figure 1, Tables 3 and 4)

Regional differences in the SOA formation process in the simple SOAG scheme compared to the VBS scheme further result in significantly smaller SOA burdens over source regions like South America, Southern Africa, Eastern China, and for present day also for the Eastern US and high northern altitudes if using the SOAG scheme (Figure 4). The SOA burden in WACCM6-SOAG is larger over other regions, including western US,

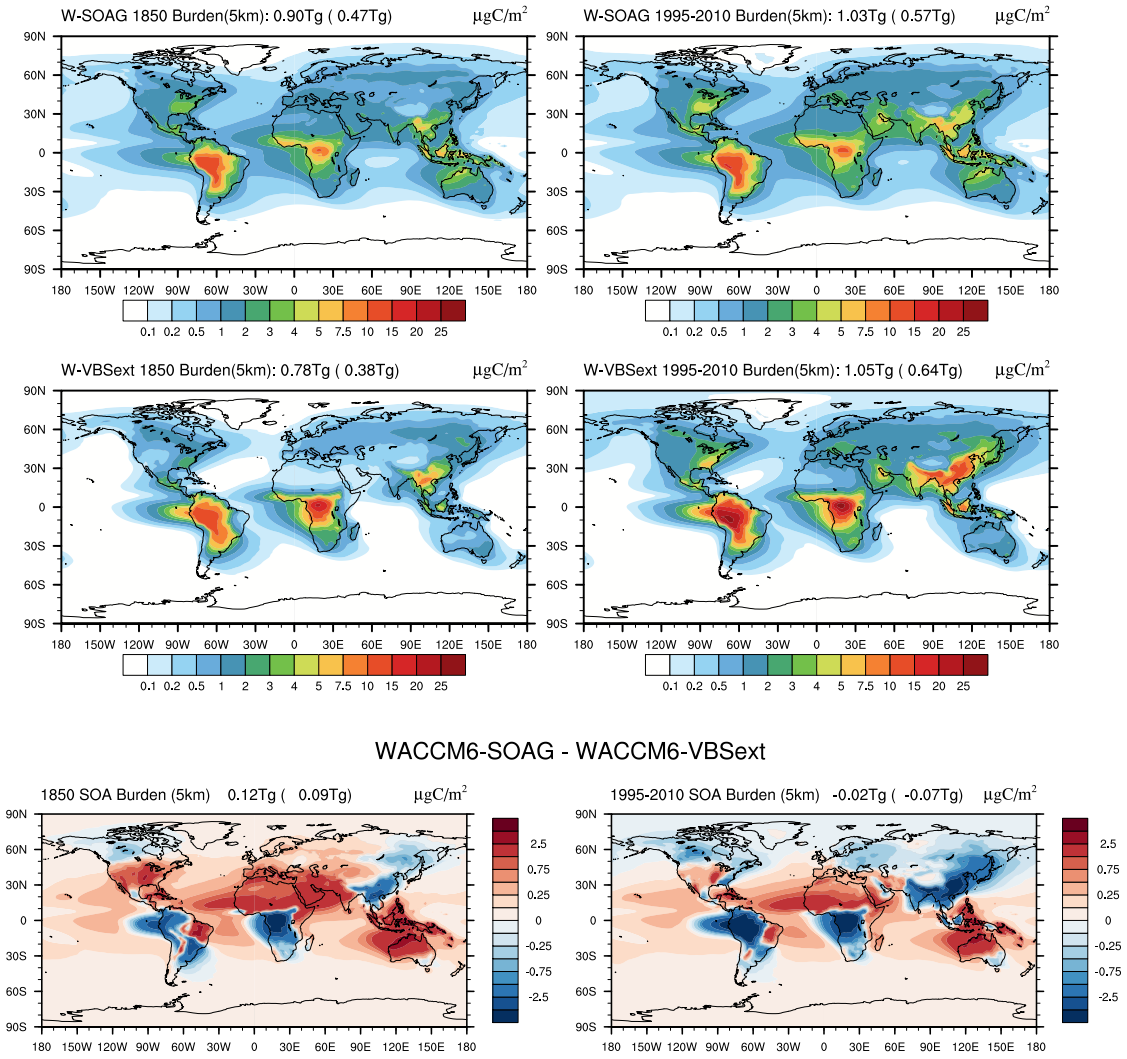

Figure 4. Annual averaged SOA burden within the lowest 5 km of the model for preindustrial conditions (left) and present day (right), and for WACCM6-SOAG (top panels) and WACCM6-VBSext (middle panels). Bottom panels: Differences between WACCM6-SOAG and WACCM6-VBSext.

Table 5. Aerosol burden separated into different modes, pre-industrial conditions

SOA	WACCM6-SOAG	WACCM6-VBSext	difference	rel diff(%)
Burden (Tg)	0.915	0.791	0.124	13.530
accumulation	0.907	0.785	0.123	13.506
Aitken	0.008	0.007	0.001	7.879
Burden (Tg) (<500hPa)	0.526	0.421	0.105	19.950
POM	WACCM6-SOAG	WACCM6-VBSext	difference	rel diff(%)
Burden (Tg)	0.517	0.405	0.112	21.597
accumulation	0.280	0.308	-0.028	-10.110
primary carbon	0.237	0.097	0.140	59.000
Burden (Tg) (<500hPa)	0.402	0.323	0.079	19.719
BC	WACCM6-SOAG	WACCM6-VBSext	difference	rel diff(%)
Burden (Tg)	0.051	0.042	0.009	17.681
accumulation	0.029	0.032	-0.003	-11.406
primary carbon	0.023	0.010	0.012	54.699
Burden (Tg) (<500hPa)	0.040	0.033	0.007	16.857
SO4	WACCM6-SOAG	WACCM6-VBSext	difference	rel diff(%)
Burden (TgS)	0.512	0.515	-0.003	-0.667
accumulation	0.330	0.353	-0.022	-6.749
Aitken	0.019	0.017	0.002	8.714
coarse	0.163	0.145	0.017	10.588
Burden (TgS) (<500hPa)	0.089	0.088	0.001	0.997

351 **Table 6.** Aerosol burden separated into different modes, 1995-2010

SOA	WACCM6-SOAG	WACCM6-VBSext	difference	rel diff(%)
Burden (Tg)	1.049	1.069	-0.019	-1.858
accumulation	1.042	1.061	-0.019	-1.788
Aitken	0.007	0.010	-0.002	-31.125
Burden (Tg) (<500hPa)	0.636	0.699	-0.063	-9.869
POM	WACCM6-SOAG	WACCM6-VBSext	difference	rel diff(%)
Burden (Tg)	0.938	0.753	0.185	19.708
accumulation	0.627	0.635	-0.008	-1.348
primary carbon	0.311	0.118	0.193	62.106
Burden (Tg) (<500hPa)	0.623	0.536	0.088	14.048
BC	WACCM6-SOAG	WACCM6-VBSext	difference	rel diff(%)
Burden (Tg)	0.149	0.134	0.015	10.121
accumulation	0.109	0.112	-0.004	-3.428
primary carbon	0.040	0.021	0.019	46.762
Burden (Tg) (<500hPa)	0.102	0.094	0.008	7.748
SO4	WACCM6-SOAG	WACCM6-VBS	difference	rel diff(%)
Burden (TgS)	0.582	0.582	-0.000	-0.060
accumulation	0.488	0.502	-0.014	-2.809
Aitken	0.014	0.013	0.001	6.343
coarse	0.080	0.068	0.012	15.566
Burden (TgS) (<500hPa)	0.303	0.303	0.000	0.136

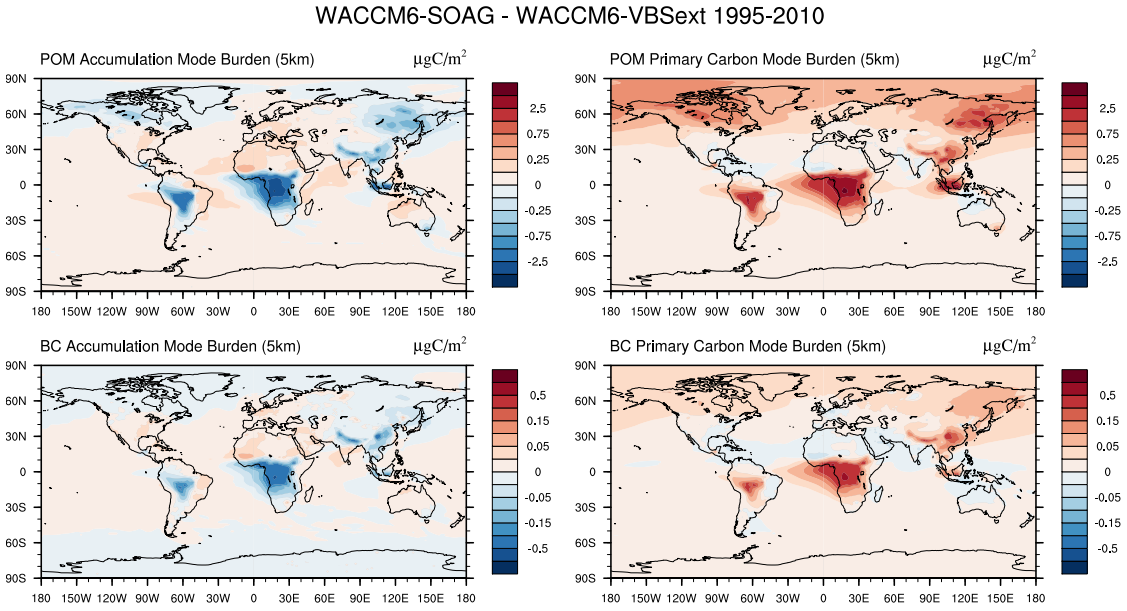

Figure 5. Differences of annual averaged POM (top) and BC (bottom) burden below 5 km between WACCM6-SOAG and WACCM6-VBSext. Left panels show the accumulation mode burden differences, right panels show differences of the primary carbon mode.

North Africa, and Australia. In contrast, differences in POM and BC between WACCM6-SOAG and WACCM6-VBSext (Figure 5) show larger burdens in WACCM6-SOAG over source regions and over high northern latitudes in the primary organic carbon mode and reductions in the accumulation mode. This is the result of the slower aging of POM and BC using the SOAG scheme.

Regional changes in aerosol mass and size between the two configurations impact Aerosol Optical Depth (AOD) and Cloud Condensation Nuclei (CCN), and therefore shortwave cloud forcing in the model (Figure 6). While the global averaged AOD values between the two approaches is unchanged (Table 7), reductions in AOD and CCN occur over SOA production regions in WACCM6-SOAG compared to WACCM6-VBSext, with implications for the regional climate. On the other hand, the larger burden of SOA, POM and BC in WACCM6-SOAG is likely responsible for the increase in AOD elsewhere. However, the increase in OA and BC burden does not lead to an increase in CCN and rather contributes to the decrease over the source regions and high northern latitudes (Figure 6, middle panel). This is, because CCN is mostly controlled by the accumulation mode, which is actually decreasing in WACCM6-SOAG compared to WACCM6-VBS. For WACCM6-

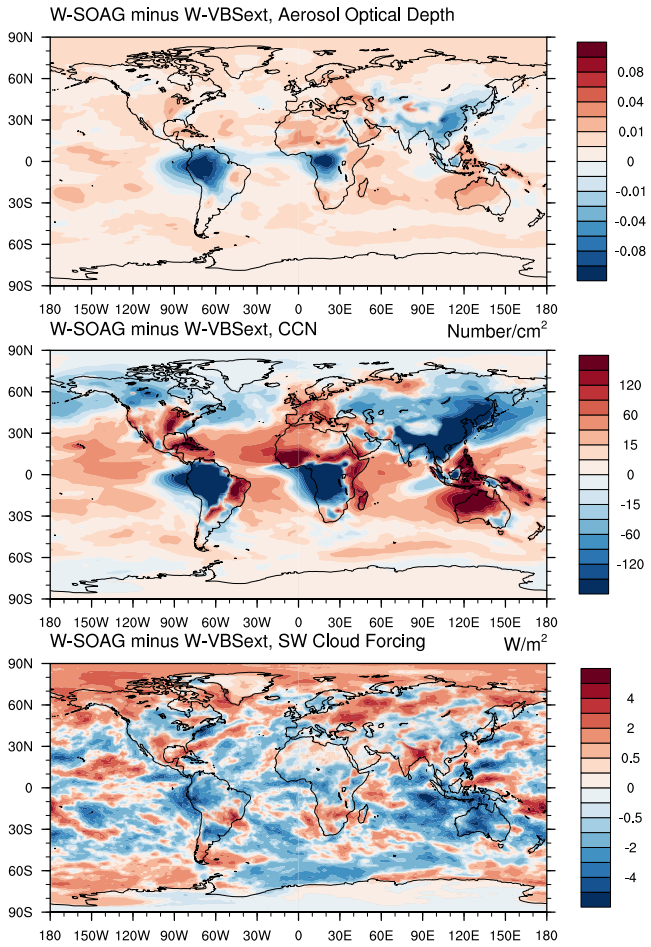

Figure 6. Differences between WACCM6-SOAG and WACCM6-VBSext for the period 1995-2010, for Aerosol Optical Depth (top), Cloud Condensation Nuclei (middle) and Short-Wave Cloud Forcing (bottom).

SOAG, about one third of the burden resides in the primary organic carbon mode for present day conditions (Table 6), which contributes to the mass, but not to CCN, while in WACCM-VBSext, more than 75% of POM and BC mass resides in the accumulation mode. The smaller burden of all aerosols in the accumulation mode results in an increase in SWCF over the Arctic (Figure 5, left panels), may contribute to the changes in the shortwave cloud forcing (SWCF) over the Arctic (Figure 6, bottom panel).

The global radiative budget, as listed in Table 7, is impacted by the regional change in SOA and the differences in POM and BC described above. Compared to WACCM6-VBSext, the top of the atmosphere radiative imbalance in WACCM6-SOAG is 0.15W/m^2 smaller for PI conditions and 0.22 W/m^2 smaller for present day. These numbers are within the standard deviation of the top of the atmosphere imbalance for the period considered and therefore not significant. However, these changes go along with a significant increase in SWCF in the simple SOAG configuration, in particular in high northern latitudes (Figure 6, bottom panel). Those changes also go along with a significant reduction in surface net shortwave radiation under clear (called FSNSC) and under cloudy (called FSNS) conditions.

In summary, differences in POM, BC and SOA burden and spacial and size distributions between the simple SOAG schemes (included in CAM6, WACCM6-SC and WACCM6-SOAG) and the more comprehensive VBS scheme result in a stronger radiative forcing of around 0.2 W/m^2 for PI and present-day conditions using the the simplified SOAG scheme. The apparent difference in SWCF in high northern latitudes is to at least some part due to changes in the OA and BC distribution between the different approaches. Resulting changes in the top of atmosphere imbalance, as well as regional AOD changes are expected to impact surface temperatures in a fully coupled simulation. The experiments performed in this study used the same sea surface temperatures for all the configurations, therefore changes in surface temperature will not be discussed.

3.2 Changes based on prognostic stratospheric sulfate aerosols and simple chemistry

Differences in radiative forcing between CAM6 and WACCM6 are not only due to the differences in the SOA description, but also due to changes in the sulfate aerosol description and chemistry. We now compare WACCM6-VBSext with the specified chem-

Table 7. Radiative quantities and aerosol burdens for WACCM6-VBS and differences between different experiments and WACCM-VBSext.

Years	Experiment	RF-TOA W/m^2	SWCF W/m^2	FSNS W/m^2	FSNSC W/m^2	AODVIS	POM Tg	BC Tg	SOA Tg	SO_4 Tg
1850 (10)	WA-VBSext	3.11 ± 0.28	-47.21 ± 0.18	166.14 ± 0.18	218.20 ± 0.09	0.125 ± 0.002	0.40	0.042	0.78	0.084
1850 (10)	WA-SOAG – WA-VBSext	-0.15	-0.30	-0.58	-0.24	0.002	0.11	0.009	0.12	-0.001
1850 (10)	WA-SC – WA-VBSext	0.04	0.19	0.06	-0.05	-0.008	0.12	0.009	0.14	-0.011
1850 (10)	CAM6 – WA-VBSext	-0.05	0.86	0.89	0.06	-0.007	0.11	0.009	0.16	-0.012
1995-2010	WA-VBSext	3.34 ± 0.54	-48.60 ± 0.46	163.41 ± 0.61	216.75 ± 0.25	0.14 ± 0.003	0.74	0.132	1.05	0.290
1995-2010	WA-SOAG – WA-VBSext	-0.22	-0.30	-0.64	-0.28	0.001	0.19	0.015	-0.02	0.00
1995-2010	WA-SC – WA-VBSext	-0.05	0.21	0.06	-0.05	-0.005	0.19	0.014	-0.01	-0.020
1995-2010	CAM6 – WA-VBSext	-0.43	0.86	0.33	-0.36	-0.002	0.20	0.015	0.02	-0.020
1995-2010	WA-NoAnthro – WA-VBSext	0.43	-0.01	0.43	0.42	-0.007	-0.33	0.00	-0.27	0.00

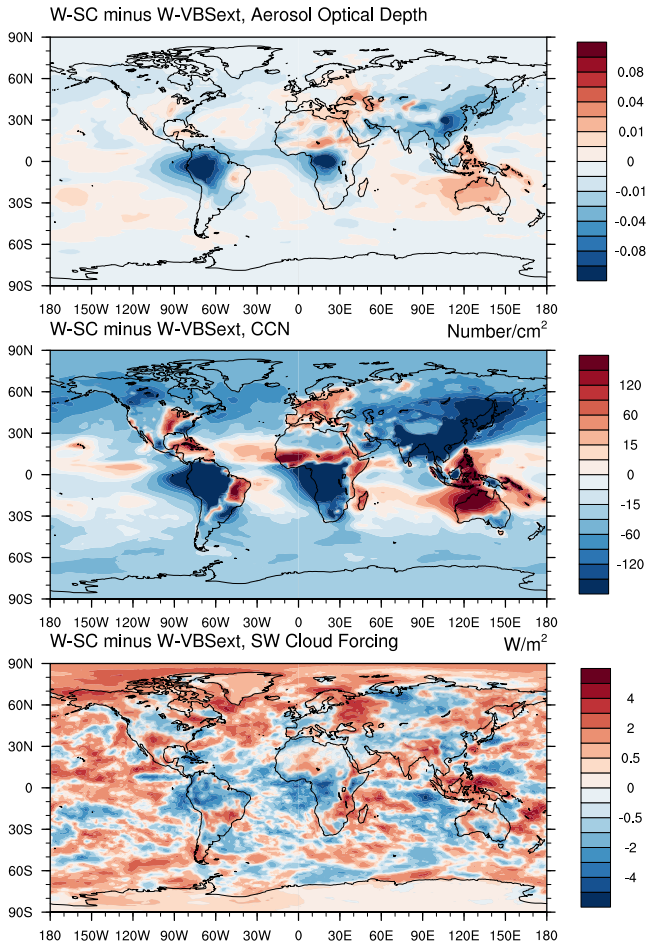

407 **Figure 7.** Differences between WACCM6-SC and WACCM6-VBSext for the period 1995-2010,
408 for Aerosol Optical Depth (top), Cloud Condensation Nuclei (middle) and Short-Wave Cloud
409 Forcing (bottom).

istry configuration (WACCM6-SC); differences include both the different SOA parameterization and differences in stratospheric sulfate aerosols. While WACCM6 and WACCM6ext include prognostic sulfates in both troposphere and stratosphere, stratospheric sulfate aerosols are prescribed in WACCM6-SC (and CAM6) and are not included in the total sulfate burden. Sulfate burdens in Figure 1 for WACCM6-SC and CAM6 do therefore not include the modal aerosol burden of stratospheric sulfates and only show the tropospheric fraction. In order to have a better comparison between results using these different approaches, we only compare the sulfate aerosol burden below 500hPa for all configurations. Nevertheless, WACCM6 configurations (with prognostic stratospheric sulfate) show a significantly larger sulfate burden below 500hPa than the other configurations and burdens vary with the amount of SO_2 input by episodic volcanic eruptions. Such eruptions inject some SO_2 directly into the troposphere in WACCM6, while more descends to the troposphere from the stratosphere. WACCM6-SC and CAM6 are lacking SO_2 emissions from volcanic eruptions, as well as OCS, accounting for their reduced tropospheric burdens.

The smaller tropospheric sulfate aerosol burden in WACCM6-SC results in reduced global AOD and increases clear sky net downwelling shortwave radiation, and in a reduction in CCN over most regions (Figure 7). Despite the large reduction in CCN, differences in the shortwave cloud forcing are only slightly different from the changes caused by the new SOA implementation (Figure 6), in particular in high northern latitudes. This indicates that differences in the SOA parameterization may be mostly responsible for these differences and are not caused by the difference in the sulfate aerosol description. These changes have been shown to have implications for climate in particular the performance of sea-ice in the model between CAM and WACCM [*Gettelman et al.*, 2019]. Nevertheless, differences in the SOA scheme and the sulfate aerosol description impact both CCN and SWCF globally. The combined differences of the reduced sulfate forcing (reduced sulfate aerosol burden) and increased forcing (0.15 W/m^2, see above) using a different SOA parameterizations between the two model versions, result in a combined small top of the atmosphere imbalance of 0.04 W/m^2 for preindustrial conditions, and -0.05W/m^2 for present day (Table 7).

3.3 Differences between high and low top versions of the model

Differences between high and low top experiments can be identified if comparing CAM6 and WACCM6-SC. Aerosol burden in those simulations are very similar for most of the aerosols, with a somewhat larger SOA burden for CAM6 compared to the WACCM6 configurations and a longer lifetime for most of the aerosols (Tables 3 and 4). Differences are attributed to reduced wet deposition of aerosols in CAM6 compared to WACCM6, which points to differences in precipitation. The slight increase in aerosol burden seems to have some effect on the SWCF, which is larger in CAM6 compared to WACCM6 for both PI and present day conditions. Other changes between WACCM6 and CAM6 are investigated in more detail in *Gettelman et al.* [2019].

3.4 Comparisons of organic aerosols to observations

Simulated present day total burdens of POM and SOA of 0.74 Tg and 1.05 Tg in WACCM6-VBSext and 0.93 Tg and 1.04 Tg for WACCM6-SOAG, respectively, are in the range of the AeroCom-II model ensemble [*Tsigaridis et al.*, 2014]. These values are smaller than what has been estimated by observations of 1.84 Tg for the SOA burden [*Spracklen et al.*, 2011]. Nevertheless, the formation of SOA from gas-to-aerosol exchange processes of $\approx$ 143 Tg per year in WACCM6-VBSext is in excellent agreement with estimates of 140 Tg per year by *Spracklen et al.* [2011] using a top-down approach constrained by a global data set of surface AMS measurements. These values are also comparable to 132 Tg per year derived in *Hodzic et al.* [2016]. However, the simulated SOA formation from WACCM6-NA without fossil fuel sources of 105 Tg per year results in only $\approx$ 38 Tg per year contribution from anthropogenic sources, which is much lower than the estimated value of 100 Tg per year by *Spracklen et al.* [2011]. Simulated PI values of 100Tg per year in WACCM6-VBSext confirm the large fraction of SOA formation from biogenic sources in the model. For WACCM6-SOAG, SOA formation reaches only around 80 Tg per year. The value of photolytic removal of SOA in WACCM6-VBSext of about 57 Tg per year is very close to estimations by *Hodzic et al.* [2016]. Other removal processes, including wet and dry deposition are 73 Tg per year and 12.5 Tg per year, respectively, which is very close to the multi-model median values of AeroCom-II models of 70 Tg per year and 13Tg per year, reported by *Tsigaridis et al.* [2014]. The resulting lifetime of 4.5 years for SOA in WACCM6 further falls right within the range of AeroCom-II model results.

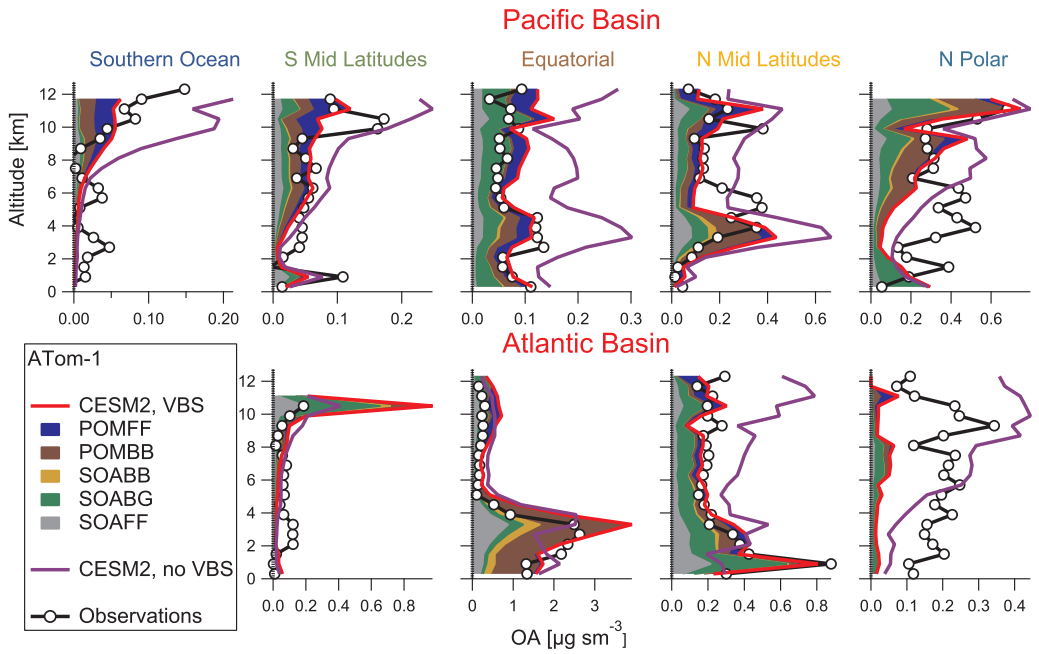

Figure 8. Comparison of regional-averaged OA vertical profiles from ATom1 measurements (black line with open circles) with two specified dynamics (SD) WACCM6 configuration, SD WACCM6-VBSext (red lines), and SD WACCM6-SOAG (purple line), indicated in the legend as CESM2, VBS, and CESM2, no VBS. Contributions from different sources for POM and SOA in the model are indicated by different colors, fossil fuel for POM (blue), biomass burning for POM (brown), biomass burning for SOA (light brown), biogenic for SOA (green), and fossil fuel for SOA (grey). Model results were interpolated to the flight track of the observations and averaged over the same region.

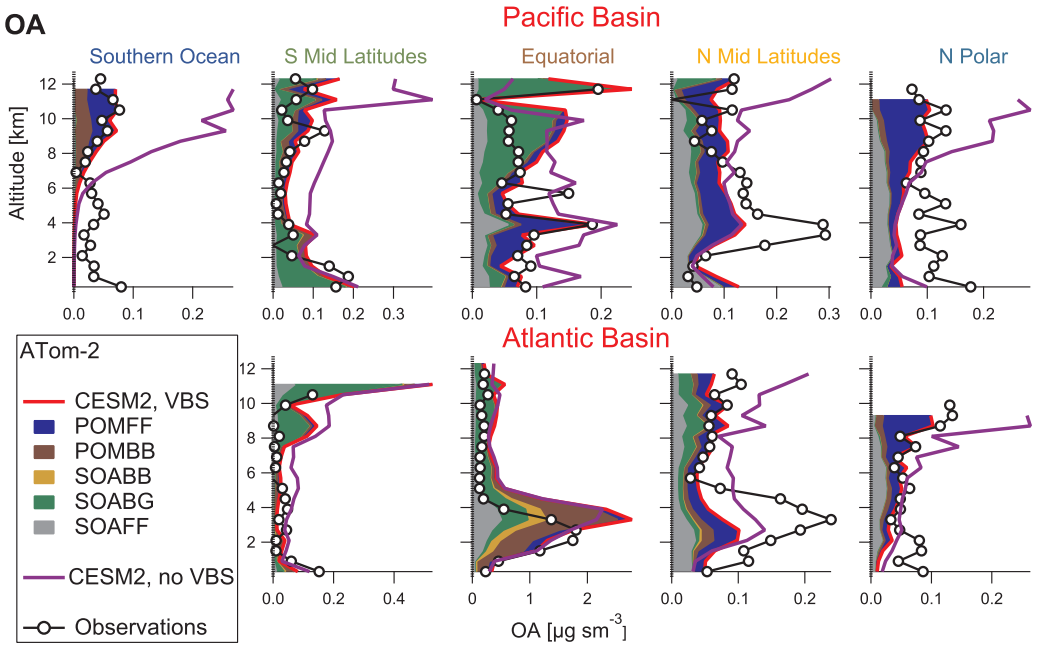

Figure 9. As Figure 12, but for ATom2 instead.

Comparisons of WACCM6 and WACCM6-SOAG to aircraft observations from the NASA ATom mission [*Wofsy et al.*, 2018] have been performed to identify improvements of the SOA parameterization. Here we focus on evaluating the performance of OA vertical distributions over different latitude regions (Figures 8 and 9). ATom sampled the marine remote troposphere in both the Atlantic and Pacific Ocean Basins from 65°S to 82°N from 0 to 12 km over four aircraft deployments. Submicron aerosol composition on board the NASA DC-8 aircraft was measured by the University of Colorado Aerodyne High-Resolution Time-of Flight Instrument (CU-HR-AMS) at 1 Hz resolution [*DeCarlo et al.*, 2006; *Canagaratna et al.*, 2007; *Nault et al.*, 2018]. Refractory black carbon was measured by the NOAA SP2 instrument, also at 1 Hz resolution [*Schwarz et al.*, 2006; *Katich et al.*, 2018]. For this work, we are focusing on the first two deployments: ATom 1 observations were taken between July and August of 2016, and ATom 2 during January and February of 2017.

To get the best comparison to the observations, WACCM6-VBSext and WACCM6-SOAG have been run with nudged GEOS5 meteorological analysis. In addition, the model has been sampled on the ATom flight track to produce output close (within 15 minutes) to the sample time of the observations. Aircraft and model results are averaged over predefined regions, to separate the characteristics of specific regions. Source contributions

of different sources for both SOA and POM from the model are indicated in different colors (Figures 8 and 9).

For most cases, OA from WACCM6-VBSext agrees very well within about 20% of the observed OA profiles for ATom 1 and 2, except for a few regions. In particular different magnitudes of OA observed between winter and summer are reproduced, including the largest OA values around the equator for the Atlantic Basin, which is caused by biomass burning smoke from the sub-Saharan African regions [*Flamant et al.*, 2018]. The model has a tendency to underpredict OA in the lower troposphere in high northern latitudes over the Pacific basin and for the Atlantic basin in summer only, which is likely an underestimation of emissions from fires or anthropogenic pollution. The model is also underestimating OA in the northern mid-latitudes in winter, potentially a result of missing anthropogenic sources. On the other hand, OA over the Pacific Basis at the equator is overestimated. In this region the model suggests a large contribution of biogenic emissions that are likely overestimated over the Amazon. Despite the very good agreement of the total OA in WACCM6-VBSext, the ratio between POM and SOA in the model does not agree well with what is known from observations. For WACCM6-SOAG, OA mixing ratios are overestimated compared to observed values by in part over a factor of two in mid- to upper troposphere and at the Equator over the Pacific Basin. This bias is removed using the new SOA parameterization in WACCM6.

The addition of the comprehensive SOA scheme in WACCM6 has resulted in a significant reduction in POM and BC burden compared to versions with the simplified SOA scheme, as discussed in Section 3.1. ATom 1 and 2 observations of BC are also compared to model results (Figures A.2. an A.3.). In general, the model overestimates BC for both WACCM6-VBSext and WACCM6-SOAG configurations especially in the mid- to upper troposphere in mid- and high latitudes. WACCM6-VBSext shows a slight improvement in this bias. *Yu et al.* [2019] have shown that wet scavenging above the cloud top in all CESM2 configurations is largely underestimated, which results in the high bias. On the other hand, WACCM6-VBSext shows much more realistic BC values in the lower troposphere (below 5km) compared to WACCM6-SOAG. This difference could have a significant effect on lower clouds and potentially affects the radiation over high latitudes, which at least in part explains differences in summer sea-ice extent between CESM2 versions with and without the comprehensive SOA scheme [*Gettelman et al.*, 2019].

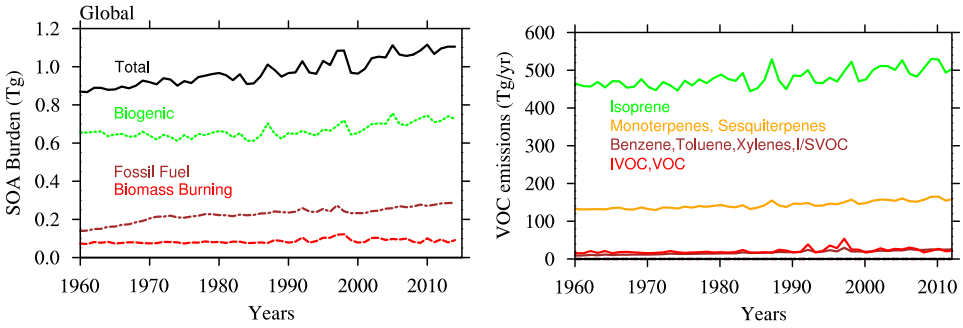

Figure 10. Left panel: Annual and global averages of total SOA burden (black) and SOA burden from different precursor sources, including biogenic (green), fossil fuel (brown), and biomass burning (red), between 1960 and 2014 derived using WACCM6-VBSext. Right panel: SOA precursor VOC emissions (in Tg per yr) of anthropogenic sources (brown), biomass buring sources (red) and biogenic sources (green and orange).

4 SOA source contributions, regional trends, and SOA anthropogenic radiative forcing

SOA source contributions have been derived using WACCM6-VBSext (Figure 10, left panel). The majority (two thirds) of the total SOA burden are produced from biogenic sources. The smallest contribution by far to the total SOA burden is from biomass burning. Both SOA burden from biogenic and fossil fuel sources are increasing between 1960 and 2014. The global increase in biogenic emissions (Figure 10, right panel) mostly from isoprene and terpene emissions is liked to increasing surface temperatures and CO_2 concentrations. The global increases in anthropogenic emissions are discussed below.

The regional distribution of OA (POM and SOA) columns in WACCM6-VBSext shows largest values over the Amazon, Central Africa, Eastern Asia, and Indonesia (Figures 11 and 12). Biogenic emissions are the largest contributor to SOA formation, in particular over the Amazon, Central Africa, Indonesia, and Australia. Over Eastern Asia, both, biogenic and fossil fuel emissions seem to be equally important for the production of SOA, with the strongest contribution over India and China. Over North America, Europe and Northern Asia, the SOA burden is relatively small and largest contributions are from fossil fuel and biogenic emissions. For POM, fossil fuel contributions are the most important sources over Eastern China, India and West Africa (Nigeria) (Figure 11). However, largest contributions are from biomass burning over Central Africa, and over the Amazon and Indonesia, while they are much smaller over Eastern China and Siberia.

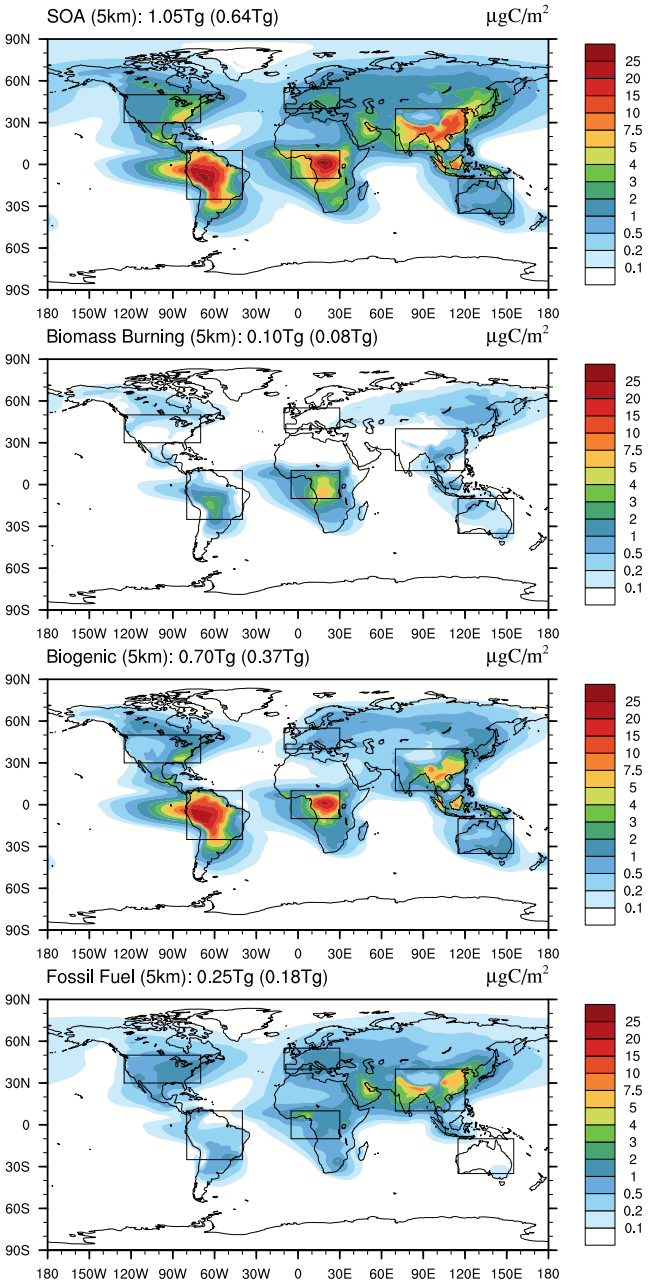

Figure 11. Annual averages of total SOA burden within the lowest 5 km of the model for WACCM6-VBSext (top panel). The lower three panels show SOA burden contributions produced by precursor emissions from biomass burning (second panel), biogenic (third panel), and fossil fuel (fourth panel). The global total SOA burden for the entire column is given on the top left of each panel, the total burden below 5km is shown in brackets. Regional areas of interest as discussed below are marked by black squares.

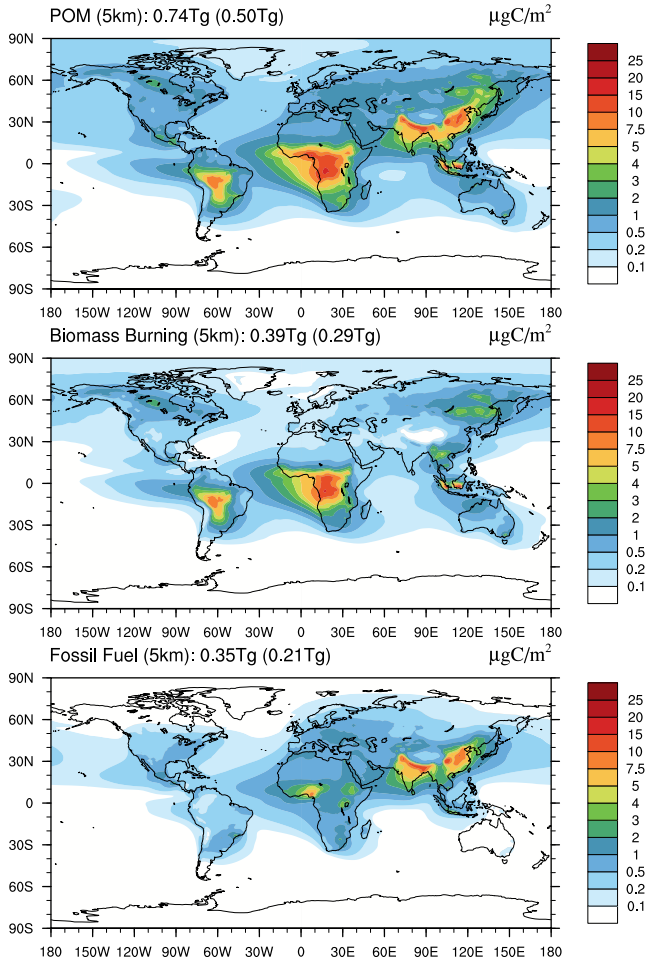

Figure 12. Annual averages of total POM burden within the lowest 5 km of the model for WACCM6-VBSext (top panel). The lower two panels show POM burden contributions produced by precursor emissions from biomass burning (second panel) and fossil fuel (third panel). The global total POM burden for the entire column is given on the top left of each panel, the total burden below 5km is shown in brackets.

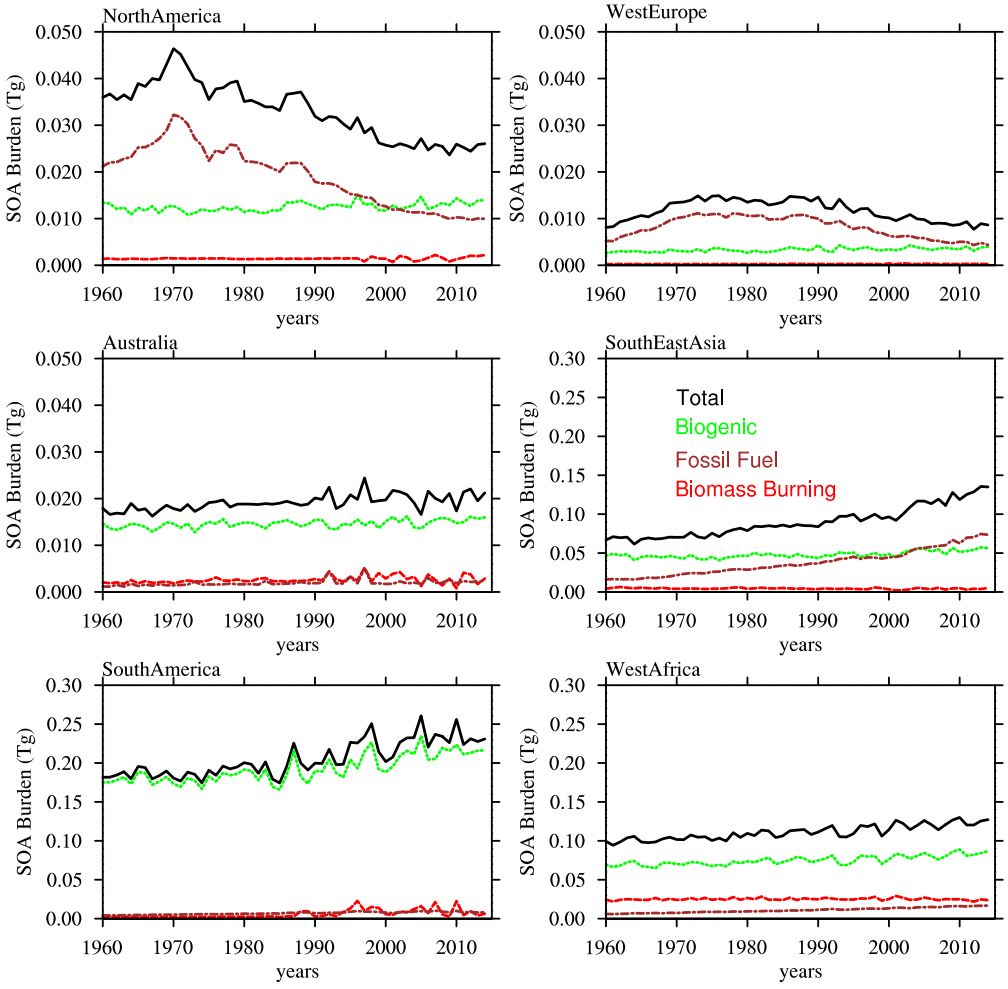

Figure 13. Annually averaged total SOA burden (black), and SOA burden from separate precursor sources, including biogenic (green), fossil fuel (brown), and biomass burning (red), averaged over six regions as indicated in Figure 8, between 1960 and 2014 derived using WACCM6-VBSext.

Regional trends of total SOA burden and from the three separate sources between 1960-2014 show changes in the importance of the source contributions with time and region (Figure 13). The SOA burden over North America, Western Europe, and Australia, is illustrated using a different y-axis range compared to the other regions for better visibility of the trends. Both North America and Western Europe show maximum fossil fuel contributions around 1970 and a steady decline from thereon, with up to 3 times larger values for North America compared to Western Europe. By around the year 2000, SOA burden from fossil fuel over Northern America is reaching below the burden produced from biogenic emissions. For Western Europe, SOA burden from fossil fuel is also approaching the amount from biogenic emissions by the end of the considered time period. Biomass burning plays a minor role over these regions. South America, Australia, and Central Africa SOA burden is dominated by the SOA production from biogenic sources, with largest total contributions in the Amazon. The increasing trend of SOA burden from biogenic sources over the Amazon (Figure 13, bottom left), is most likely due to the effects of the changes in surface temperature and changing CO_2 concentrations on biogenic emissions in the model, which have been increasing (Figure 10, right panel).

SOA burden over Southeast Asia is dominated by biogenic precursor emissions until around the year 2000. After that, fossil fuel emissions are the dominant contributor to SOA. The production of SOA from fossil fuel emissions is about 5 times as large as the anthropogenic amount produced over North America, and 10 times larger compared to Europe by around 2014 (the end of the simulations). SOA from biogenic emissions has been increasing in the last 20 years or so over Southeast Asia. The SOA production from biomass burning sources are largest over West to Central Africa. This region also shows a positive trend of SOA from biogenic and fossil fuel sources. In addition, contributions from fossil fuel emissions are increasing and almost reaching the levels of biomass burning in 2014. Since about 1990, SOA burden from fossil fuel over West and Central Africa is larger than anthropogenic contributions for North America, with still increasing trends.

The total SOA trend (Figure 1, left panel) is dominated by the strong increase in SOA from fossil fuel precursor emissions over Eastern Asia and West and Central Africa, as well as the increase in biogenic emissions (as described above). To identify the importance of anthropogenic source contributions to total SOA burden, trends, as well as radiation, we performed the WACCM-NA sensitivity simulation. The trend in total aerosol

burden from this simulation is shown in Figure 1, green lines, and Table 3, right most column. The total SOA burden is reduced by more than 25% and the POM burden by more than 45%. Other aerosols, including SO_4 and BC are not significantly impacted by the removal of anthropogenic SOA and POM.

The combined impact of fossil fuel POM emissions and fossil fuel precursor emissions to the formation of SOA on the top of the atmosphere imbalance for present day (1995-2010) is -0.43 W/m^2. Similar changes are simulated for all sky and clear sky downwelling shortwave net radiation at the surface (Table 7). The variability of the top of the imbalance is rather large, but differences between WACCM6-NA and WACCM6-VBSext in the net shortwave downwelling radiation at the surface for clear and full sky are 0.42 W/m^2 and 0.43 W/m^2, respectively, and are significant and persistence throughout the entire time series between 1960-2014. On the other hand, the shortwave cloud forcing does not show any significant changes between the simulations. This indicates a minor indirect effect of the anthropogenic contribution of OA in the model. The derived total radiative forcing of OA is on the higher end of the forcing reported in AeroCom-II models [*Tsigaridis and Kanakidou*, 2018].

5 Discussion and Conclusions

In this study, we discussed differences in chemistry and aerosol parameterizations for different CESM2 model configurations. Despite using the same physics description, WACCM6 and CAM6-chem include a more comprehensive and interactive SOA parameterization following the approach by *Hodzic et al.* [2016]. WACCM6-SC and CAM6 use a simplified SOA parameterization, which has been already used in CESM(CAM5) [*Liu et al.*, 2012, 2016]. The more comprehensive SOA scheme in WACCM6 uses the VBS approach for SOA formation and includes updated removals and interactions with biogenic emissions through the coupling to MEGAN2.1. With this parameterization, source contributions of different SOA and POM precursors from biomass burning, anthropogenic and biogenic emissions (for SOA only) can be identified. In parallel, prognostic stratospheric sulfates have been added in WACCM6 and CAM6-chem [*Mills et al.*, 2017]. For the purpose of identifying changes and effects on radiation based on the different SOA parameterizations as well as other differences, a comparison of different WACCM6 and CAM6 versions has been performed. Those include the standard WACCM6 version, a WACCM6-VBSext version, which explicitly simulates OA source contributions, a WACCM6-

SC version, which uses simplified chemistry and aerosols, and WACCM6-SOAG, which includes the same chemistry and aerosols as WACCM6, but uses the simplified SOA parameterization.

Due to the improved interactions between biogenic emissions and SOA formation, WACCM6 describes stronger trends of SOA between 1960 and 2014 than what is estimated using the simplified SOA scheme. These differences point to a different SOA response to climate change between WACCM6 and WACCM6-SOAG and therefore CAM6, with potential implication for climate sensitivity. Furthermore, differences in SOA in particular over source regions result in an increased aging of BC and POM in WACCM6, which causes changes in wet and dry removal, aerosol mass and size distribution. These differences between WACCM6 and WACCM6-SOAG impact AOD and shortwave cloud forcing in particular over the source regions and northern high latitudes. Potential changes in sea-ice between WACCM6 and CAM6 [*Gettelman et al.*, 2019] are likely a result of changes in the aerosol description in the two models.

The new parameterization in WACCM6 performs very well with regard to SOA formation in comparison to observational estimates from *Spracklen et al.* [2011]. Estimates of OA burden, removal and lifetime are very close to the multi-model mean estimate from the AeroCom-II model ensemble [*Tsigaridis et al.*, 2014]. OA mixing ratios further agree within 20% with ATom 1 and 2 aircraft observations over the remote troposphere. CESM2 configurations without comprehensive chemistry show a high bias in OA in particular in the upper troposphere. However, in general all CESM2 configurations show reasonable OA burdens compared to AeroCom-II models. Nevertheless, shortcomings in the partitioning between POM and SOA contributions to the total OA mass compared to observations even with the more comprehensive SOA parameterization in WACCM6 have to be investigated in future studies and more work has to be done to improve the transition between POM and SOA.

Shortcomings in the model still exist, including the omission of representing high NO_x conditions in the comprehensive SOA parameterization. Furthermore, the experimental evidence suggests that under low-NO_x conditions (typical of forest regions), isoprene SOA is mainly formed due to multiphase chemistry from isoprene epoxydiols (IEPOX-SOA) in aqueous particles, and that pure gas-phase VBS parameterizations are not appropriate to represent this irreversible IEPOX uptake into aqueous SOA. *Jo et al.* [2019]

showed that the isoprene SOA concentrations predicted with the VBS were substantially lower over remote regions, and somewhat higher over isoprene source regions than those predicted with the IEPOX-SOA parameterization [*Marais et al.*, 2016]. *Shrivastava et al.* [2019] estimated that over the Amazon forest $\approx 30\%$ of biogenic SOA (formed through oxidation of both isoprene and terpenes) was IEPOX-SOA formed through multiphase chemistry versus 70% from pure gas-phase chemistry and partitioning represented by the VBS approach. Similarly, *Hu et al.* [2015] reported that $\approx 34\%$ of OA could be attributed to IEPOX-SOA over the pristine Amazon forest. This chemistry will be included in the future model versions and is expected to increase the SOA global burden and reduce some of the SOA concentrations over the Amazon source region. Additional future improvements for the model include the addition of brown carbon [*Brown et al.*, 2018] and updates in below cloud-top scavenging. These will likely improve the high bias of BC (and POM) in mid-to upper troposphere as pointed out by *Yu et al.* [2019]. Both these updates are expected to further impact radiative effects in CESM2.

Acknowledgments

We thank Rebecca Schwantes and Rebecca R. Buchholz for helpful comments to the manuscript, as well as Rebecca R. Buchholz for producing QFED emissions files. The CESM project is supported primarily by the National Science Foundation (NSF). This material is based upon work supported by the National Center for Atmospheric Research, which is a major facility sponsored by the NSF under Cooperative Agreement No. 1852977. Computing and data storage resources, including the Cheyenne supercomputer (doi:10.5065/D6RX99HX), were provided by the Computational and Information Systems Laboratory (CISL) at NCAR. All simulations were carried out on the Cheyenne high-performance computing platform https://www2.cisl.ucar.edu/user-support/acknowledging-ncarcisl, and are available to the community via the Earth System Grid.

References

Aumont, B., S. Szopa, and S. Madronich (2005), Modelling the evolution of organic carbon during its gas-phase tropospheric oxidation: development of an explicit model based on a self generating approach, *Atmospheric Chemistry and Physics*, *5*(9), 2497–2517, doi:10.5194/acp-5-2497-2005.

Brown, H., X. Liu, Y. Feng, Y. Jiang, M. Wu, Z. Lu, C. Wu, S. Murphy, and R. Pokhrel (2018), Radiative effect and climate impacts of brown carbon with the Community Atmosphere Model (CAM5), *Atmospheric Chemistry and Physics*, *18*(24), 17,745–17,768, doi:10.5194/acp-18-17745-2018.

Canagaratna, M. R., J. T. J. T. Jayne, J. L. Jimenez, J. D. Allan, M. R. Alfarra, Q. Q. Zhang, T. B. Onasch, F. Drewnick, H. Coe, A. M. Middlebrook, A. Delia, L. R. Williams, A. M. Trimborn, M. J. Northway, P. F. DeCarlo, C. E. Kolb, P. Davidovits, and D. R. Worsnop (2007), Chemical and microphysical characterization of ambient aerosols with the Aerodyne Aerosol Mass Spectrometer, *Mass Spectrom. Rev.*, *262*(2), 185–222, doi:10.1002/mas.

Carslaw, K. S., L. A. Lee, C. L. Reddington, K. J. Pringle, A. Rap, P. M. Forster, G. W. Mann, D. V. Spracklen, M. T. Woodhouse, L. A. Regayre, and J. R. Pierce (2013), Large contribution of natural aerosols to uncertainty in indirect forcing, *Nature*, *503*(7474), 67–71, doi:10.1038/nature12674.

Chin, M., P. Ginoux, S. Kinne, O. Torres, B. N. Holben, B. N. Duncan, R. V. Martin, J. A. Logan, A. Higurashi, and T. Nakajima (2002), Tropospheric Aerosol Optical Thickness from the GOCART Model and Comparisons with Satellite and Sun Photometer Measurements, *Journal of the Atmospheric Sciences*, *59*(3), 461–483, doi:10.1175/1520-0469(2002)059¡0461:TAOTFT¿2.0.CO;2.

Colarco, P., A. Da Silva, M. Chin, and T. Diehl (2010), Online simulations of global aerosol distributions in the NASA GEOS-4 model and comparisons to satellite and ground-based aerosol optical depth, *Journal of Geophysical Research Atmospheres*, *115*(14), doi:10.1029/2009JD012820.

Darmenov, A. S., A. da Silvia, and R. D. Koster (2015), The Quick Fire Emissions Dataset (QFED): Documentation of Versions 2.1, 2.2 and 2.4. Volume 38; Technical Report Series on Global Modeling and Data Assimilation, *Tech. rep.*, NASA Goddard Space Flight Center, Greenbelt, MD, United States.

DeCarlo, P. F., J. R. Kimmel, A. Trimborn, M. J. Northway, J. T. Jayne, A. C. Aiken, M. Gonin, K. Fuhrer, T. Horvath, K. S. Docherty, D. R. Worsnop, and J. L. Jimenez (2006), Field-Deployable, High-Resolution, Time-of-Flight Aerosol Mass Spectrometer, *Analytical Chemistry*, *78*(24), 8281–8289, doi:10.1021/ac061249n.

Donahue, N. M., A. L. Robinson, C. O. Stanier, and S. N. Pandis (2006), Coupled Partitioning, Dilution, and Chemical Aging of Semivolatile Organics, *Environmental Science & Technology*, *40*(8), 2635–2643, doi:10.1021/es052297c.

Flamant, C., P. Knippertz, A. H. Fink, A. Akpo, B. Brooks, C. J. Chiu, H. Coe, S. Danuor, M. Evans, O. Jegede, N. Kalthoff, A. Konaré, C. Liousse, F. Lohou, C. Mari, H. Schlager, A. Schwarzenboeck, B. Adler, L. Amekudzi, J. Aryee, M. Ayoola, A. M. Batenburg, G. Bessardon, S. Borrmann, J. Brito, K. Bower, F. Burnet, V. Catoire, A. Colomb, C. Denjean, K. Fosu-Amankwah, P. G. Hill, J. Lee, M. Lothon, M. Maranan, J. Marsham, R. Meynadier, J.-B. Ngamini, P. Rosenberg, D. Sauer, V. Smith, G. Stratmann, J. W. Taylor, C. Voigt, and V. Yoboué (2018), The Dynamics–Aerosol–Chemistry–Cloud Interactions in West Africa Field Campaign: Overview and Research Highlights, *Bulletin of the American Meteorological Society*, *99*(1), 83–104, doi:10.1175/BAMS-D-16-0256.1.

Gentner, D. R., G. Isaacman, D. R. Worton, A. W. H. Chan, T. R. Dallmann, L. Davis, S. Liu, D. A. Day, L. M. Russell, K. R. Wilson, R. Weber, A. Guha, R. A. Harley, and A. H. Goldstein (2012), Elucidating secondary organic aerosol from diesel and gasoline vehicles through detailed characterization of organic carbon emissions, *Proceedings of the National Academy of Sciences*, *109*(45), 18,318–18,323, doi:10.1073/pnas.1212272109.

Gettelman, A., M. J. Miils, D. E. Kinnison, R. Garcia, A. Smith, D. R. Marsh, S. Tilmes., F. Vitt, C. G. Bardeen, J. McInerny, H.-L. Liu, S. C. Solomon, M. Polvani, L., K. Emmons., L., J.-F. Lamarque, J. H. Richter, S. Glanville, A., J. T. Bacmeister, A. S. Phillips, R. B. Neale, I. R. Simpson, K. DuVivier, A., A. Hodzic, and W. J. Randel (2019), The Whole Atmosphere Community Climate Model Version 6 (WACCM6), *Journal of Geophysical Research Atmospheres*.

Guenther, a. B., X. Jiang, C. L. Heald, T. Sakulyanontvittaya, T. Duhl, L. K. Emmons, and X. Wang (2012), The Model of Emissions of Gases and Aerosols from Nature version 2.1 (MEGAN2.1): an extended and updated framework for modeling biogenic emissions, *Geoscientific Model Development*, *5*(6), 1471–1492, doi:10.5194/gmd-5-1471-2012.

Hallquist, M., J. C. Wenger, U. Baltensperger, Y. Rudich, D. Simpson, M. Claeys, and J. Dommen (2009), Hallquist et al., 2009, *Atmospheric Chemistry and Physics*, *9*(November 2008), 5155–5236, doi:10.5194/acp-9-5155-2009.

Heald, C. L., H. Coe, J. L. Jimenez, R. J. Weber, R. Bahreini, A. M. Middlebrook, L. M. Russell, M. Jolleys, T. M. Fu, J. D. Allan, K. N. Bower, G. Capes, J. Crosier, W. T. Morgan, N. H. Robinson, P. I. Williams, M. J. Cubison, P. F. Decarlo, and E. J. Dunlea (2011), Exploring the vertical profile of atmospheric organic aerosol: Comparing 17 aircraft field campaigns with a global model, *Atmospheric Chemistry and Physics*, *11*(24), 12,676–12,696, doi:10.5194/acp-11-12673-2011.

Hodzic, A., and J. P. Duvel (2018), Impact of Biomass Burning Aerosols on the Diurnal Cycle of Convective Clouds and Precipitation Over a Tropical Island, *Journal of Geophysical Research: Atmospheres*, *123*(2), 1017–1036, doi:10.1002/2017JD027521.

Hodzic, A., J. L. Jimenez, S. Madronich, M. R. Canagaratna, P. F. DeCarlo, L. Kleinman, and J. Fast (2010), Modeling organic aerosols in a megacity: potential contribution of semi-volatile and intermediate volatility primary organic compounds to secondary organic aerosol formation, *Atmospheric Chemistry and Physics*, *10*(12), 5491–5514, doi:10.5194/acp-10-5491-2010.

Hodzic, A., B. Aumont, C. Knote, J. Lee-Taylor, S. Madronich, and G. Tyndall (2014), Volatility dependence of Henry's law constants of condensable organics: Application to estimate depositional loss of secondary organic aerosols, *Geophysical Research Letters*, *41*(13), 4795–4804, doi:10.1002/2014GL060649.

Hodzic, A., S. Madronich, P. S. Kasibhatla, G. Tyndall, B. Aumont, J. L. Jimenez, J. Lee-Taylor, and J. Orlando (2015), Organic photolysis reactions in tropospheric aerosols: Effect on secondary organic aerosol formation and lifetime, *Atmospheric Chemistry and Physics*, *15*(16), 9253–9269, doi:10.5194/acp-15-9253-2015.

Hodzic, A., P. S. Kasibhatla, D. S. Jo, C. D. Cappa, J. L. Jimenez, S. Madronich, and R. J. Park (2016), Rethinking the global secondary organic aerosol (SOA) budget: Stronger production, faster removal, shorter lifetime, *Atmospheric Chemistry and Physics*, *16*(12), 7917–7941, doi:10.5194/acp-16-7917-2016.

Hoesly, R. M., S. J. Smith, L. Feng, Z. Klimont, G. Janssens-Maenhout, T. Pitkanen, J. J. Seibert, L. Vu, R. J. Andres, R. M. Bolt, T. C. Bond, L. Dawidowski, N. Kholod, J.-i. Kurokawa, M. Li, L. Liu, Z. Lu, M. C. P. Moura, P. R. O'Rourke, and Q. Zhang (2018), Historical (1750–2014) anthropogenic emissions of reactive gases and aerosols from the Community Emissions Data System

(CEDS), *Geoscientific Model Development*, *11*(1), 369–408, doi:10.5194/gmd-11-369-2018.

Hu, W. W., P. Campuzano-Jost, B. B. Palm, D. A. Day, A. M. Ortega, P. L. Hayes, J. E. Krechmer, Q. Chen, M. Kuwata, Y. J. Liu, S. S. de Sá, K. McKinney, S. T. Martin, M. Hu, S. H. Budisulistiorini, M. Riva, J. D. Surratt, J. M. St. Clair, G. Isaacman-Van Wertz, L. D. Yee, A. H. Goldstein, S. Carbone, J. Brito, P. Artaxo, J. A. de Gouw, A. Koss, A. Wisthaler, T. Mikoviny, T. Karl, L. Kaser, W. Jud, A. Hansel, K. S. Docherty, M. L. Alexander, N. H. Robinson, H. Coe, J. D. Allan, M. R. Canagaratna, F. Paulot, and J. L. Jimenez (2015), Characterization of a real-time tracer for isoprene epoxydiols-derived secondary organic aerosol (IEPOX-SOA) from aerosol mass spectrometer measurements, *Atmospheric Chemistry and Physics*, *15*(20), 11,807–11,833, doi:10.5194/acp-15-11807-2015.

Jathar, S. H., T. D. Gordon, C. J. Hennigan, H. O. T. Pye, G. Pouliot, P. J. Adams, N. M. Donahue, and A. L. Robinson (2014), Unspeciated organic emissions from combustion sources and their influence on the secondary organic aerosol budget in the United States, *Proceedings of the National Academy of Sciences*, *111*(29), 10,473–10,478, doi:10.1073/pnas.1323740111.

Jo, D. S., A. Hodzic, L. K. Emmons, E. A. Marais, Z. Peng, B. A. Nault, W. Hu, P. Campuzano-Jost, and J. L. Jimenez (2019), A simplified parameterization of isoprene-epoxydiol-derived secondary organic aerosol (IEPOX-SOA) for global chemistry and climate models, *Geoscientific Model Development Discussions*, pp. 1–36, doi:10.5194/gmd-2019-9.

Katich, J. M., B. H. Samset, T. P. Bui, M. Dollner, K. D. Froyd, P. Campuzano-Jost, B. A. Nault, J. C. Schroder, B. Weinzierl, and J. P. Schwarz (2018), Strong Contrast in Remote Black Carbon Aerosol Loadings Between the Atlantic and Pacific Basins, *Journal of Geophysical Research: Atmospheres*, *123*(23), 13,386–13,395, doi:10.1029/2018JD029206.

Kleindienst, T. E., M. Jaoui, M. Lewandowski, J. H. Offenberg, C. W. Lewis, P. V. Bhave, and E. O. Edney (2007), Estimates of the contributions of biogenic and anthropogenic hydrocarbons to secondary organic aerosol at a southeastern US location, *Atmospheric Environment*, *41*(37), 8288–8300, doi:10.1016/j.atmosenv.2007.06.045.

Knote, C., A. Hodzic, J. L. Jimenez, R. Volkamer, J. J. Orlando, S. Baidar, J. Brioude, J. Fast, D. R. Gentner, A. H. Goldstein, P. L. Hayes, W. B. Knighton, H. Oetjen, A. Setyan, H. Stark, R. Thalman, G. Tyndall, R. Washenfelder, E. Waxman, and Q. Zhang (2014), Simulation of semi-explicit mechanisms of SOA formation from glyoxal in aerosol in a 3-D model, *Atmospheric Chemistry and Physics*, *14*(12), 6213–6239, doi:10.5194/acp-14-6213-2014.

Liu, X., R. C. Easter, S. J. Ghan, R. Zaveri, P. Rasch, X. Shi, J.-F. Lamarque, a. Gettelman, H. Morrison, F. Vitt, a. Conley, S. Park, R. Neale, C. Hannay, a. M. L. Ekman, P. Hess, N. Mahowald, W. Collins, M. J. Iacono, C. S. Bretherton, M. G. Flanner, and D. Mitchell (2012), Toward a minimal representation of aerosols in climate models: description and evaluation in the Community Atmosphere Model CAM5, *Geoscientific Model Development*, *5*(3), 709–739, doi:10.5194/gmd-5-709-2012.

Liu, X., P. L. Ma, H. Wang, S. Tilmes, B. Singh, R. C. Easter, S. J. Ghan, and P. J. Rasch (2016), Description and evaluation of a new four-mode version of the Modal Aerosol Module (MAM4) within version 5.3 of the Community Atmosphere Model, *Geoscientific Model Development*, *9*(2), 505–522, doi:10.5194/gmd-9-505-2016.

Marais, E. A., D. J. Jacob, J. L. Jimenez, P. Campuzano-Jost, D. A. Day, W. Hu, J. Krechmer, L. Zhu, P. S. Kim, C. C. Miller, J. A. Fisher, K. Travis, K. Yu, T. F. Hanisco, G. M. Wolfe, H. L. Arkinson, H. O. T. Pye, K. D. Froyd, J. Liao, and V. F. McNeill (2016), Aqueous-phase mechanism for secondary organic aerosol formation from isoprene: application to the southeast United States and co-benefit of SO₂ emission controls, *Atmospheric Chemistry and Physics*, *16*(3), 1603–1618, doi:10.5194/acp-16-1603-2016.

Mills, M. J., J. H. Richter, S. Tilmes, B. Kravitz, D. G. MacMartin, A. A. Glanville, J. J. Tribbia, J.-F. Lamarque, F. Vitt, A. Schmidt, A. Gettelman, C. Hannay, J. T. Bacmeister, and D. E. Kinnison (2017), Radiative and chemical response to interactive stratospheric sulfate aerosols in fully coupled CESM1(WACCM), *Journal of Geophysical Research: Atmospheres*, *122*(23), doi:10.1002/2017JD027006.

Nault, B. A., P. Campuzano-Jost, D. A. Day, J. C. Schroder, B. Anderson, A. J. Beyersdorf, D. R. Blake, W. H. Brune, Y. Choi, C. A. Corr, J. A. de Gouw, J. Dibb, J. P. DiGangi, G. S. Diskin, A. Fried, L. G. Huey, M. J. Kim, C. J.

Knote, K. D. Lamb, T. Lee, T. Park, S. E. Pusede, E. Scheuer, K. L. Thornhill, J.-H. Woo, and J. L. Jimenez (2018), Secondary organic aerosol production from local emissions dominates the organic aerosol budget over Seoul, South Korea, during KORUS-AQ, *Atmospheric Chemistry and Physics*, *18*(24), 17,769–17,800, doi:10.5194/acp-18-17769-2018.

Neely, R. R., I., and A. Schmidt (2016), VolcanEESM: Global volcanic sulphur dioxide (SO2) emissions database from 1850 to present—Version 1.0, doi: 10.5285/76ebdc0b-0eed-4f70- b89e-55e606bcd568.

Ng, N. L., J. H. Kroll, A. W. H. Chan, P. S. Chhabra, R. C. Flagan, and J. H. Seinfeld (2007), Secondary organic aerosol formation from m-xylene, toluene, and benzene, *Atmospheric Chemistry and Physics*, *7*(14), 3909–3922, doi:10.5194/acp-7-3909-2007.

Odum, J. R., Thorsten Hoffmann, Frank Bowman, Don Collins, Richard C. Flagan, and John H. Seinfeld (1996), Gas/Particle Partitioning and Secondary Organic Aerosol Yields, *Environmental Science and Technology*, *30*(8), 2580–2585, doi: 10.1021/ES950943+.

Pandis, S. N., S. E. Paulson, J. H. Seinfeld, and R. C. Flagan (1991), Aerosol formation in the photooxidation of isoprene and β-pinene, *Atmospheric Environment Part A, General Topics*, *25*(5-6), 997–1008, doi:10.1016/0960-1686(91)90141-S.

Pye, H. O., and J. H. Seinfeld (2010), A global perspective on aerosol from low-volatility organic compounds, *Atmospheric Chemistry and Physics*, *10*(9), 4377–4401, doi:10.5194/acp-10-4377-2010.

Robinson, A. L., N. M. Donahue, M. K. Shrivastava, E. A. Weitkamp, A. M. Sage, A. P. Grieshop, T. E. Lane, J. R. Pierce, and S. N. Pandis (2007), Rethinking organic aerosols: Semivolatile emissions and photochemical aging, *Science*, *315*(5816), 1259–1262, doi:10.1126/science.1133061.

Sayer, A. M., L. A. Munchak, N. C. Hsu, R. C. Levy, C. Bettenhausen, and M.-J. Jeong (2014), MODIS Collection 6 aerosol products: Comparison between Aqua's e-Deep Blue, Dark Target, and "merged" data sets, and usage recommendations, *Journal of Geophysical Research: Atmospheres*, *119*(24), 13,965–13,989, doi:10.1002/2014JD022453.

Schwarz, J. P., R. S. Gao, D. W. Fahey, D. S. Thomson, L. A. Watts, J. C. Wilson, J. M. Reeves, M. Darbeheshti, D. G. Baumgardner, G. L. Kok, S. H. Chung,

M. Schulz, J. Hendricks, A. Lauer, B. Kärcher, J. G. Slowik, K. H. Rosenlof, T. L. Thompson, A. O. Langford, M. Loewenstein, and K. C. Aikin (2006), Single-particle measurements of midlatitude black carbon and light-scattering aerosols from the boundary layer to the lower stratosphere, *Journal of Geophysical Research*, *111*(D16), D16,207, doi:10.1029/2006JD007076.

Shrivastava, M., A. Zelenyuk, D. Imre, R. Easter, J. Beranek, R. A. Zaveri, and J. Fast (2013), Implications of low volatility SOA and gas-phase fragmentation reactions on SOA loadings and their spatial and temporal evolution in the atmosphere, *Journal of Geophysical Research Atmospheres*, *118*(8), 3328–3342, doi:10.1002/jgrd.50160.

Shrivastava, M., R. C. Easter, X. Liu, A. Zelenyuk, B. Singh, K. Zhang, P.-L. Ma, D. Chand, S. Ghan, J. L. Jimenez, Q. Zhang, J. Fast, P. J. Rasch, and P. Tiitta (2015), Global transformation and fate of SOA: Implications of low-volatility SOA and gas-phase fragmentation reactions, *Journal of Geophysical Research: Atmospheres*, *120*(9), 4169–4195, doi:10.1002/2014JD022563.

Shrivastava, M., C. D. Cappa, J. Fan, A. H. Goldstein, A. B. Guenther, J. L. Jimenez, C. Kuang, A. Laskin, S. T. Martin, N. L. Ng, T. Petaja, J. R. Pierce, P. J. Rasch, P. Roldin, J. H. Seinfeld, J. Shilling, J. N. Smith, J. A. Thornton, R. Volkamer, J. Wang, D. R. Worsnop, R. A. Zaveri, A. Zelenyuk, and Q. Zhang (2017), Recent advances in understanding secondary organic aerosol: Implications for global climate forcing, *Reviews of Geophysics*, *55*(2), 509–559, doi:10.1002/2016RG000540.

Shrivastava, M., M. O. Andreae, P. Artaxo, H. M. J. Barbosa, L. K. Berg, J. Brito, J. Ching, R. C. Easter, J. Fan, J. D. Fast, Z. Feng, J. D. Fuentes, M. Glasius, A. H. Goldstein, E. G. Alves, H. Gomes, D. Gu, A. Guenther, S. H. Jathar, S. Kim, Y. Liu, S. Lou, S. T. Martin, V. F. McNeill, A. Medeiros, S. S. de Sá, J. E. Shilling, S. R. Springston, R. A. F. Souza, J. A. Thornton, G. Isaacman-VanWertz, L. D. Yee, R. Ynoue, R. A. Zaveri, A. Zelenyuk, and C. Zhao (2019), Urban pollution greatly enhances formation of natural aerosols over the Amazon rainforest, *Nature Communications*, *10*(1), 1046, doi:10.1038/s41467-019-08909-4.

Spracklen, D. V., J. L. Jimenez, K. S. Carslaw, D. R. Worsnop, M. J. Evans, G. W. Mann, Q. Zhang, M. R. Canagaratna, J. Allan, H. Coe, G. McFiggans, A. Rap, and P. Forster (2011), Aerosol mass spectrometer constraint on the global sec-

ondary organic aerosol budget, *Atmospheric Chemistry and Physics*, *11*(23), 12,109–12,136, doi:10.5194/acp-11-12109-2011.

Tilmes, S., B. M. Sanderson, and B. C. O'Neill (2016), Climate impacts of geoengineering in a delayed mitigation scenario, *Geophysical Research Letters*, *43*(15), 8222–8229, doi:10.1002/2016GL070122.

Tsigaridis, K., and M. Kanakidou (2018), The Present and Future of Secondary Organic Aerosol Direct Forcing on Climate, *Current Climate Change Reports*, *4*(2), 84–98, doi:10.1007/s40641-018-0092-3.

Tsigaridis, K., N. Daskalakis, M. Kanakidou, P. J. Adams, P. Artaxo, R. Bahadur, Y. Balkanski, S. E. Bauer, N. Bellouin, a. Benedetti, T. Bergman, T. K. Berntsen, J. P. Beukes, H. Bian, K. S. Carslaw, M. Chin, G. Curci, T. Diehl, R. C. Easter, S. J. Ghan, S. L. Gong, a. Hodzic, C. R. Hoyle, T. Iversen, S. Jathar, J. L. Jimenez, J. W. Kaiser, a. Kirkevåg, D. Koch, H. Kokkola, Y. H. Lee, G. Lin, X. Liu, G. Luo, X. Ma, G. W. Mann, N. Mihalopoulos, J.-J. Morcrette, J.-F. Müller, G. Myhre, S. Myriokefalitakis, N. L. Ng, D. O'Donnell, J. E. Penner, L. Pozzoli, K. J. Pringle, L. M. Russell, M. Schulz, J. Sciare, Ø. Seland, D. T. Shindell, S. Sillman, R. B. Skeie, D. Spracklen, T. Stavrakou, S. D. Steenrod, T. Takemura, P. Tiitta, S. Tilmes, H. Tost, T. van Noije, P. G. van Zyl, K. von Salzen, F. Yu, Z. Wang, R. a. Zaveri, H. Zhang, K. Zhang, Q. Zhang, and X. Zhang (2014), The AeroCom evaluation and intercomparison of organic aerosol in global models, *Atmospheric Chemistry and Physics*, *14*(19), 10,845–10,895, doi:10.5194/acp-14-10845-2014.

Tsimpidi, A. P., V. A. Karydis, M. Zavala, W. Lei, L. Molina, I. M. Ulbrich, J. L. Jimenez, and S. N. Pandis (2010), Evaluation of the volatility basis-set approach for the simulation of organic aerosol formation in the Mexico City metropolitan area, *Atmospheric Chemistry and Physics*, *10*(2), 525–546, doi:10.5194/acp-10-525-2010.

Wiedinmyer, C., S. K. Akagi, R. J. Yokelson, L. K. Emmons, J. A. Al-Saadi, J. J. Orlando, and A. J. Soja (2011), The Fire INventory from NCAR (FINN): a high resolution global model to estimate the emissions from open burning, *Geoscientific Model Development*, *4*(3), 625–641, doi:10.5194/gmd-4-625-2011.

Wofsy, S. (2018), ATom: Merged Atmospheric Chemistry, Trace Gases, and Aerosols, *ORNL Distributed Active Archive Center*, doi:

964 doi.org/10.3334/ornldaac/1581.

965 Yu, P., K. D. Froyd, R. W. Portmann, O. B. Toon, S. R. Freitas, C. G. Bardeen,
966 C. Brock, T. Fan, R.-S. Gao, J. M. Katich, A. Kupc, S. Liu, C. Maloney, D. M.
967 Murphy, K. H. Rosenlof, G. Schill, J. P. Schwarz, and C. Williamson (2019), Ef-
968 ficient In-Cloud Removal of Aerosols by Deep Convection, *Geophysical Research*
969 *Letters*, *46*(2), 1061–1069, doi:10.1029/2018GL080544.

970 Zhang, X., C. D. Cappa, S. H. Jathar, R. C. McVay, J. J. Ensberg, M. J. Kleeman,
971 and J. H. Seinfeld (2014), Influence of vapor wall loss in laboratory chambers
972 on yields of secondary organic aerosol, *Proceedings of the National Academy of*
973 *Sciences*, *111*(16), 5802–5807, doi:10.1073/pnas.1404727111.

974 Zhang, Y., H. Forrister, J. Liu, J. Dibb, B. Anderson, J. P. Schwarz, A. E. Perring,
975 J. L. Jimenez, P. Campuzano-Jost, Y. Wang, A. Nenes, and R. J. Weber (2017),
976 Top-of-atmosphere radiative forcing affected by brown carbon in the upper tropo-
977 sphere, *Nature Geoscience*, *10*(7), 486–489, doi:10.1038/ngeo2960.

A: Comparisons of AOD between WACCM6 and MODIS satellite observations

For a comparison of AOD, we use satellite observations from the Moderate Resolution Imaging Spectroradiometer (MODIS) sensors on the Terra and Aqua platforms [*Sayer et al.*, 2014]. The retrievals from the two instruments agree on many features of annually averaged AOD between 2002-2014, including largest values of AOD over Southeast Asia, and Northern India, as well as over West and Central Africa. Lowest values over land occur over Australia. Smaller differences are apparent over the subtropical ocean (Figure A.1., first row). For comparisons to the model, we use an average of both satellite instruments.

AOD from WACCM6-VBSext and WACCM6-SOAG (Figure A.1., second row) show slight differences over the SOA source regions, consistent with Figures 5 and 7. In comparison to observations, the largest overestimation of AOD occurs over Saharan Africa, and over Asian desert regions in both model configurations. In addition, AOD in WACCM6 is larger over the subtropical ocean and in the Southern Ocean. These differences are likely a result of potential overestimation of sea salt emissions in the model, but may be also caused by too little rainfall in particular over the subtropical oceans. Furthermore, the observations may misrepresent AOD over desert areas. Differences in the subtropical areas may be caused from comparing clear sky observations with full sky model results. The model further underestimates higher AOD values over Indonesia, likely due to the underestimation for biomass burning over these regions.

Comparisons over SOA source regions indicate that largest differences in AOD between the different SOA schemes occur over the Amazon, Central Africa forest regions, and Eastern China. Both model versions strongly underestimate AOD over Eastern China, with only a very small improvement in WACCM6-VBSext, pointing to an underestimation of aerosol emissions and aerosol precursor emissions. Differences over Central Africa have only been slightly improved in WACCM6-VBSext compared to WACCM6-SOAG. Over the Amazon, WACCM6-SOAG shows a slight underestimation of AOD, while WACCM6-VBSext slightly overestimates AOD. The overestimation of AOD over Australia in WACCM6-SOAG has been somewhat improved in the WACCM6-VBSext.

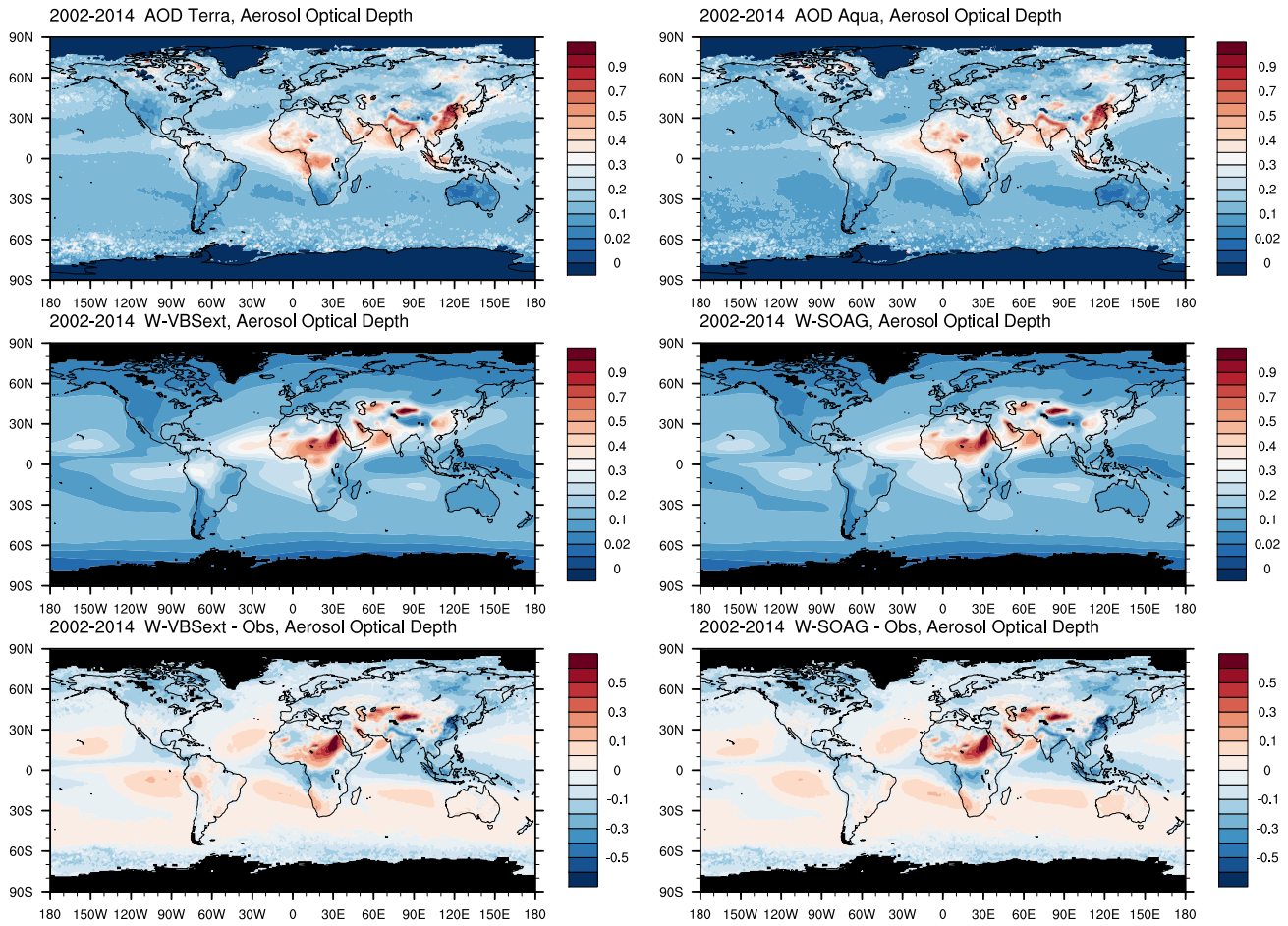

Figure A.1. Aerosol Optical Depth in the visible (550nm), averaged between 2002 and 2014 from MODIS observations, TERRA (top left), and AQUA (top right), and from WACCM6-VBSext (middle left) and WACCM6-SOAG (middle right). Bottom panels show differences between WACCM6-VBSext and the observations (average between AQUA and TERRA) (left) and between WACCM6-SOAG and observations (right).

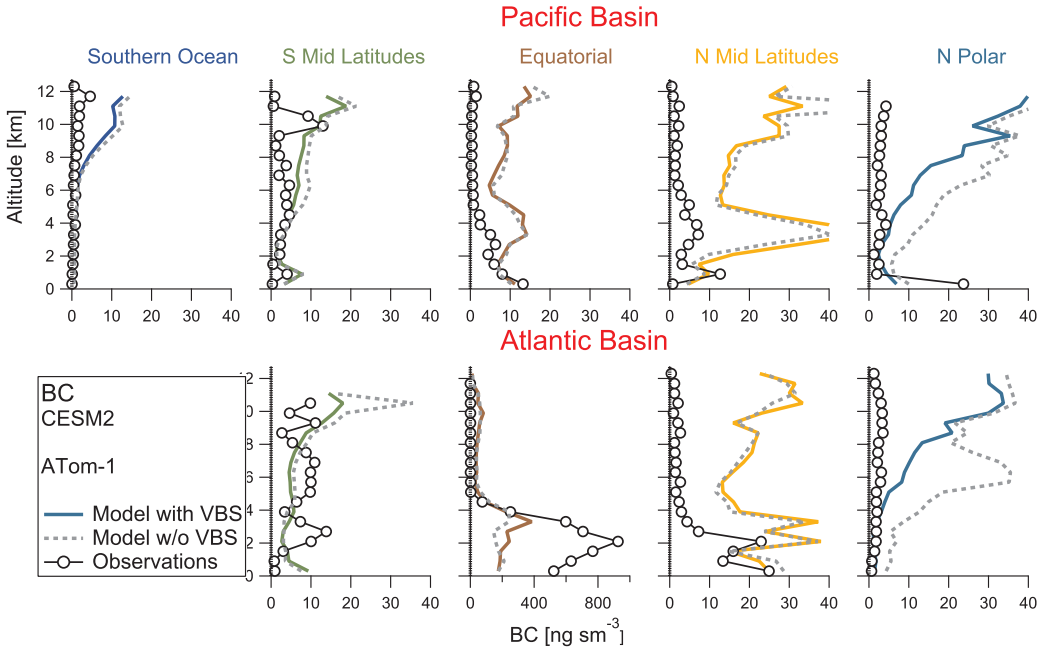

1013 **Figure A.2.** As Figure 8, but comparing BC instead of POM and SOA. WACCM6-VBSext
1014 results are shown as solid colored lines, WACCM6-SOAG results are shown as dashed lines.

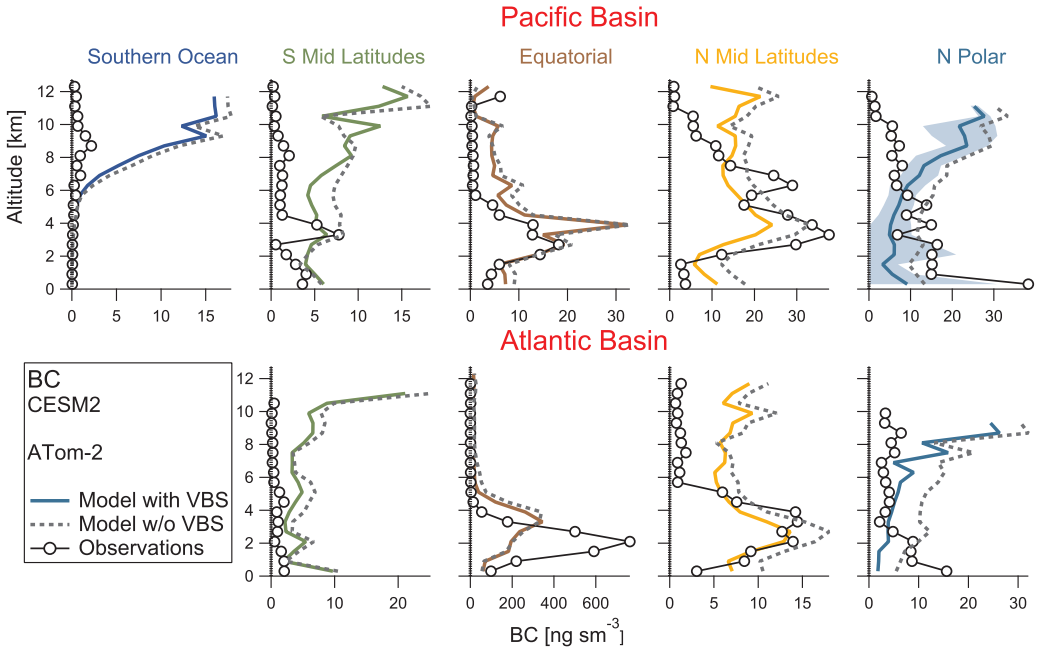

1015 **Figure A.3.** As Figure A.2, but for ATom2 instead.